J. Fluid Mech. (2021), *vol*. 917, A19, doi:10.1017/jfm.2021.274

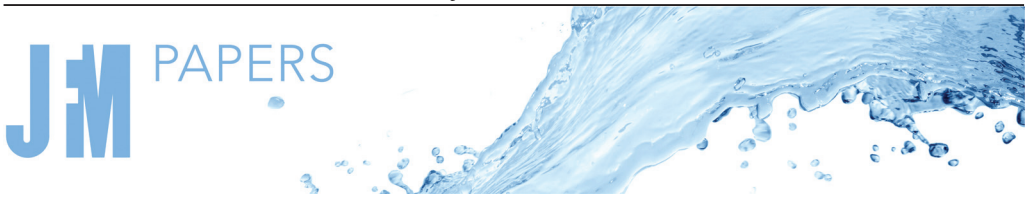

Interactions of waves with a body floating in an open water channel confined by two semi-infinite ice sheets

Zhi Fu Li[1], **Guo Xiong Wu**[2,†] **and Kang Ren**[2]

[1]School of Naval Architecture and Ocean Engineering, Jiangsu University of Science and Technology, Zhenjiang 212003, PR China

[2]Department of Mechanical Engineering, University College London, Torrington Place, London WC1E 7JE, UK

(Received 17 August 2020; revised 4 February 2021; accepted 16 March 2021)

Wave radiation and diffraction problems of a body floating in an open water channel confined by two semi-infinite ice sheets are considered. The linearized velocity potential theory is used for fluid flow and a thin elastic plate model is adopted for the ice sheet. The Green function, which satisfies all the boundary conditions apart from that on the body surface, is first derived. This is obtained through applying Fourier transform in the longitudinal direction of the channel, and matched eigenfunction expansions in the transverse plane. With the help of the derived Green function, the boundary integral equation of the potential is derived and it is shown that the integrations over all other boundaries, including the bottom of the fluid, free surface, ice sheet, ice edge as well as far field will be zero, and only the body surface has to be retained. This allows the problem to be solved through discretization of the body surface only. Detailed results for hydrodynamic forces are provided, which are generally highly oscillatory owing to complex wave–body–channel interaction and body–body interaction. In depth investigations are made for the waves confined in a channel, which does not decay at infinity. Through this, a detailed analysis is presented on how the wave generated by a body will affect the other bodies even when they are far apart.

Key words: ice sheets, wave–structure interactions, channel flow

1. Introduction

The subject of wave interaction with a floating structure owing to radiation and diffraction is of considerable significance in ocean engineering for better design and safe operation, as well as environmental protection. In general, the ocean is treated as infinitely large,

† Email address for correspondence: g.wu@ucl.ac.uk

and the wave generated by the oscillatory motion of the structure or by its disturbance to an incident wave propagates outwards to infinity. However, there are many other cases in which the fluid region is confined or the fluid surface is not entirely free. In such a case, the wave radiated or diffracted by the body will be fully or partially reflected back to the body. This makes the interaction of a body with an external environment more complex.

A notable example of a structure in a confined water region is a channel. This problem is also related to the experimental set-up for an offshore platform in a wave tank. Early work to investigate the tank wall effect includes that by Eatock Taylor & Hung (1985) on a vertical cylinder, who placed a number of cylinders at the mirror image positions formed by the two sidewalls. Yeung & Sphaier (1989) also considered the problem of a truncated vertical circular cylinder in a channel. Their formulation used an infinite array of cylinders arranged in a plane perpendicular to the channel, and the tank wall effect, in particular its natural mode effect, was captured more accurately as a large number of cylinders could be used. A different method was used by Linton & Evans (1992), who constructed the velocity potential which satisfied the wall condition directly. This allowed the far-field wave in the channel away from the cylinder to be modelled accurately, and the trapped modes (Ursell 1951) for cylinders in a channel were captured. Wu (1998) considered a fully submerged sphere in an arbitrary position of the channel through the multipole expansion. It was found that in many cases the frequency corresponding to the trapped mode could be very close to the natural frequency. The sphere problem was also considered by Ursell (1999), who constructed the velocity potential in an integral form. For a more realistic structure with a complicated shape, the integral equation approach based on the Green function can be used. Linton (1999) derived an alternative representation of the Green function for the channel, which could be calculated more efficiently. Newman (2016) compared three numerical approaches to include the tank wave effect, i.e. the mirror image, inclusion of the sidewall in the integral equation, and the free surface Green function satisfying the wall conditions. The results from the first two approaches became less accurate when the waves became longer, as the effects of the truncation in the mirror images or the tank wall in the integral equation became more important. Through the third method, Newman (2017) further provided trapped wave modes for several bodies either fixed or freely floating in the channel.

A related problem is an open water channel confined between two semi-infinite ice sheets, an example of which is that created by an icebreaker for the navigation of commercial ships (Appolonov *et al.* 2013). This has become an increasingly popular topic in the context of Arctic engineering. Different from the tank problem described previously, where the impermeable condition on sidewalls will force the wave to fully reflect back, the waves can pass into the region below the ice sheets. A relatively thin ice sheet can be treated as an elastic plate (Robin 1963; Squire *et al.* 1988). The plate will be set into motion, which will, in turn, create a flexural gravity wave. As the free surface wave and flexural gravity wave propagate in different media, which are reflected by their different dispersion relationships, the disturbed wave can be partially reflected back to the body. This makes the wave–body interaction more complex. Through linear velocity potential theory for fluid flow and thin elastic plate model for ice deflection, Chung & Linton (2005) solved the problem of incoming wave from the region below the ice sheet and then passing through the channel using a residual calculus technique. Through Wiener–Hopf and residual calculus techniques, Williams & Squire (2006) considered the problem of three connected ice sheets with the first and last sheets to be semi-infinite, and an open water channel could be modelled by setting the thickness of middle ice sheet zero. A free surface in confined region can also be seen through a polynya in the three-dimensional

(3-D) problem. This was solved, for example, by Bennetts & Williams (2010) and the results showed that the polynya shape could have a significant effect on the diffracted wave field.

For a body inside the fluid confined by the ice sheet, Sturova (2015) considered a two-dimensional (2-D) problem of wave radiation by a body submerged in the free surface channel through boundary integral equations. For a body floating on the channel surface, Ren, Wu & Thomas (2016) obtained the solution for a rectangle through the matched eigenfunction expansions. Li, Shi & Wu (2018*a*) developed a hybrid numerical scheme for an arbitrary shaped body, which combined eigenfunction expansions under ice sheets and boundary integral equation in the channel. Based on the solution for a body in open water and that for an ice channel without a body, Li, Shi & Wu (2017) provided a solution for a body in a wide channel, and explicit equations for the hydrodynamic forces and motion responses were obtained. Although the solution was based on wide-spacing approximations, the results were in very good agreement with those without the approximation. Through these explicit equations, the mechanism for oscillatory behaviours of the results were uncovered.

For the 3-D problems, Ren, Wu & Ji (2018) considered a vertical circular cylinder in a polynya with circular shape through the series expansion. For a general 3-D problem with a practical structure and arbitrary polynya edge shape, its solution through conventional numerical methods becomes a major challenge. One of the reasons is that the commonly used Green function in ocean engineering, which allows the discretization of the structure surface only, is very difficult to construct. Another reason is the fifth derivative on the ice sheet is not easy to compute numerically. Therefore, Li, Shi & Wu (2020*a*) developed a hybrid method for this problem, in which a series of integral equations under the ice sheet were constructed and coupled with the inner boundary integral equation through an orthogonal inner product. The solution procedure is highly efficient if the polynya is finite, and is effective even when there is more than one polynya or more than one structure. However, the method is less effective for an infinitely long channel. In addition, apart from a different methodology is required, there are some different physics features of the waves in the channel and their effect on the body motions need to be better understood. In particular, it has been observed by Porter (2018) that there could be waves trapped in the channel, which do not propagate into infinity beneath the ice sheet. The implication of this is that owing to a structure the wave may continuously propagate along the channel and affect other structures at relatively large distance away.

In this work, we develop a method that is effective for this type of channel problem. Through detailed analysis and numerical results, we acquire some in-depth understanding of the wave–body interaction in a channel confined between ice sheets. The differential equation (2.2) is first converted into an integral equation through the Green function. This may seem to be conventional for the velocity potential that satisfies the Laplace equation. However, in general, the integral equation involves the full boundary of the fluid domain, which in this case is infinite. Thus, in the free surface problem, the Green function which satisfies the boundary condition on all other surfaces apart from that on the body surface is usually derived first (Wehausen & Laitone 1960). As a result, it can then be shown that other boundaries in the integral equation can be removed apart from the body surface. The same principle may be used here. However, the derivation is not trivial and is far more complicated than the free surface problem. The Green function is obtained through taking the Fourier transform in the direction along the channel, and matched eigenfunction expansions are applied in the transverse plane. Through the Green function, those waves which may be trapped in the channel are identified and captured. With this derived Green

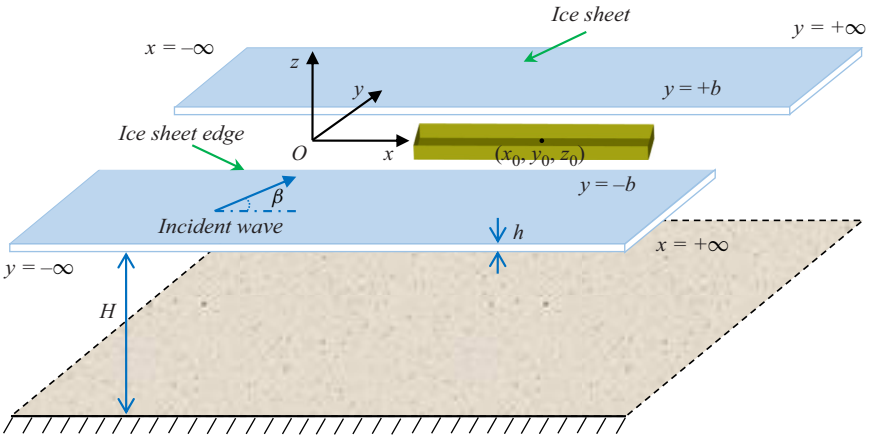

Figure 1. Coordinate system and sketch of the problem.

function, it is then further shown that as in the free surface problem the other boundaries in the integral equation can indeed be removed, only the body surface needs to be retained. Numerical discretization is then applied, through which the solution are obtained. From the solution, the complex wave–channel–body interaction is investigated, together with the body–body interaction.

The paper is organized as follows. The mathematical model is formulated in § 2, and the governing equation for ice deflection together with the free ice edge conditions are described. In § 3.1 the velocity potential due to an oscillating source or the Green function is derived, based on which the boundary integral equation for the disturbed velocity potentials is constructed in § 3.2, and the formula for the hydrodynamic forces are also provided. Results are presented and discussed in § 4, followed by the conclusion in § 5. In Appendix A, the special case for ice sheet with a zero thickness is given, whereas in Appendix B the boundary integral equation for the disturbed velocity potential is derived.

2. Mathematical model

The interaction of waves with an arbitrarily shaped body floating in an open water channel is sketched in figure 1. To describe the problem, a Cartesian coordinate system O–xyz is defined, with the O–xy plane being the undisturbed mean free water surface and the z-axis pointing vertically upwards. The channel is confined by two semi-infinite ice sheets bounded by $y = \pm b$, respectively. Following Squire (2011) and others, the ice sheet is modelled as a thin elastic plate with the associated properties, Young's modulus E, Poisson's ratio ν, density ρ_i and thickness h, being assumed to be constant and its draught effect being ignored. The motion of the body is assumed to be excited by an incident wave, which propagates from infinity from an angle β with the positive x-axis.

The fluid with density ρ_w and constant depth H is assumed to be inviscid, incompressible and homogeneous, and its motion to be irrotational. Thus, the velocity potential Φ can be introduced to describe the fluid flow. When the amplitudes of wave motion and body motion are small compared with the wavelength and the dimension of the body, the linearized velocity potential theory can be further used. For sinusoidal motion

in time with radian frequency ω, the total velocity potential can be written as

$$\Phi(x, y, z, t) = \mathrm{Re}\left[\eta_0\phi_0(x, y, z)\,\mathrm{e}^{\mathrm{i}\omega t} + \sum_{j=1}^{6} \mathrm{i}\omega\eta_j\phi_j(x, y, z)\,\mathrm{e}^{\mathrm{i}\omega t}\right], \tag{2.1}$$

where $\phi_0 = \phi_I + \phi_D$ is the scattering potential with ϕ_I and ϕ_D as the incident and diffracted potentials, respectively, η_0 is the amplitude of the incident wave and ϕ_j is the radiation potential owing to the jth mode of body motion in six degrees of freedom with complex amplitude η_j. Here, η_j $(j = 1, 2, 3)$ are for the translational modes along x, y and z directions, respectively, whereas η_j $(j = 4, 5, 6)$ are for the corresponding rotational modes. The conservation of mass requires that the velocity potential ϕ_j $(j = 0, \ldots, 6)$ should satisfy the Laplace equation throughout the fluid, or

$$\nabla^2\phi_j + \frac{\partial^2\phi_j}{\partial z^2} = 0, \tag{2.2}$$

where

$$\nabla^2 = \frac{\partial^2}{\partial x^2} + \frac{\partial^2}{\partial y^2}, \tag{2.3}$$

is the Laplacian in the horizontal plane. In the water channel, the combination of linearized dynamic and kinematic free surface boundary conditions provides

$$-\omega^2\phi_j + g\frac{\partial\phi_j}{\partial z} = 0 \quad (|y| \leqslant b - 0 \text{ and } z = 0), \tag{2.4}$$

where g is the acceleration due to gravity. It is assumed that there is no gap between ice sheet and water surface. This gives

$$\frac{\partial W}{\partial t} = \frac{\partial\Phi}{\partial z} \quad (|y| \geqslant b + 0 \text{ and } z = 0), \tag{2.5}$$

where W is the deflection of the ice sheet. Similar to (2.1), we may write W as

$$W(x, y, t) = \mathrm{Re}\left[\eta_0 w_0(x, y)\,\mathrm{e}^{\mathrm{i}\omega t} + \sum_{j=1}^{6} \mathrm{i}\omega\eta_j w_j(x, y)\,\mathrm{e}^{\mathrm{i}\omega t}\right], \tag{2.6}$$

with

$$w_j = \frac{1}{\mathrm{i}\omega}\left.\frac{\partial\phi_j}{\partial z}\right|_{z=0}. \tag{2.7}$$

This, combined with the dynamic condition on the interface, gives

$$\left(L\nabla^4 + \rho_w g - m_i\omega^2\right)\frac{\partial\phi_j}{\partial z} - \rho_w\omega^2\phi_j = 0 \quad (|y| \geqslant b + 0 \text{ and } z = 0), \tag{2.8}$$

where $L = Eh^3/[12(1 - \nu^2)]$ and $m_i = \rho_i h$ are the effective flexural rigidity and mass per unit area of the ice sheet, respectively. Here, it should be noted that in (2.4) and (2.8), $b - 0$ and $b + 0$ indicate that the ice edge is approached from the channel side and ice

sheet side, respectively. Zero bending moment and shear force conditions are imposed at the ice edge, or (Timoshenko & Woinowsky 1959)

$$\mathcal{B}\left(\frac{\partial\phi_j}{\partial z}\right)=0 \quad \text{and} \quad \mathcal{S}\left(\frac{\partial\phi_j}{\partial z}\right)=0 \quad (|y|=b+0 \text{ and } z=0), \tag{2.9}$$

for $j=0,\ldots,6$, where the operators $\mathcal{B}$ and $\mathcal{S}$ are respectively defined as

$$\mathcal{B}=\frac{\partial^2}{\partial y^2}+\nu\frac{\partial^2}{\partial x^2}, \tag{2.10}$$

$$\mathcal{S}=\frac{\partial}{\partial y}\left[\frac{\partial^2}{\partial y^2}+(2-\nu)\frac{\partial^2}{\partial x^2}\right]. \tag{2.11}$$

The impermeable condition on the mean wetted body surface S_B can be written as

$$\frac{\partial\phi_j}{\partial n}=n_j \quad \text{and} \quad \frac{\partial\phi_D}{\partial n}=-\frac{\partial\phi_I}{\partial n} \quad (j=1,\ldots,6), \tag{2.12}$$

where $(n_1,n_2,n_3)=\boldsymbol{n}$ are the components related to the translational modes, with $\boldsymbol{n}$ as the unit normal vector pointing into the body, $(n_4,n_5,n_6)=(\boldsymbol{r}-\boldsymbol{r}_0)\times\boldsymbol{n}$ are those related to the rotational modes with $\boldsymbol{r}$ being the position vector measured from the origin and $\boldsymbol{r}_0$ being the vector to the rotational centre (x_0,y_0,z_0). On the flat seabed, we have

$$\frac{\partial\phi_j}{\partial z}=0 \quad (z=-H), \tag{2.13}$$

for $j=0,\ldots,6$. At infinity, the radiation condition requires that the radiated and diffracted waves should propagate outwards.

3. Solution procedure

3.1. *Green function for an open water channel confined by two semi-infinite ice sheets*

To solve the boundary value problem for the disturbed velocity potential, we may first seek the corresponding Green function $G(p,q)$ which is defined as the velocity potential at field point $p(x,y,z)$ owing to a source at point $q(\xi,\eta,\zeta)$. Here, G should satisfy the following governing equation

$$\nabla^2 G+\frac{\partial^2 G}{\partial z^2}=-4\pi\delta(x-\xi)\delta(y-\eta)\delta(z-\zeta), \tag{3.1}$$

throughout the fluid, and the same boundary conditions in (2.4), (2.8), (2.9), (2.13) and the radiation condition. Here, $\delta(x)$ is the Dirac delta function.

To derive G, we use the Fourier transform

$$\tilde{G}=\frac{1}{2\pi}\int_{-\infty}^{+\infty} G\,\mathrm{e}^{-\mathrm{i}\alpha x}\,\mathrm{d}x. \tag{3.2}$$

It should be mentioned that G is an oscillatory function as $|x|\to+\infty$. One way to perform Fourier transform for this kind of function is to introduce a small negative imaginary part in the radian frequency ω (Lighthill 1978). In the inverse Fourier transform, the imaginary part will tend to zero. The integration path at the singularities are deflected and the radiation condition is then satisfied automatically. This procedure is used by

Li, Wu & Ji (2018*b*). Alternatively, we do not introduce the imaginary part in ω. Once $\tilde{G}$ is derived and its inverse transform is performed, the integration path at the singularities will be decided by the radiation condition, as can be seen later. The governing equation (3.1) for G then becomes, after Fourier transform,

$$-\alpha^2\tilde{G}+\frac{\partial^2\tilde{G}}{\partial y^2}+\frac{\partial^2\tilde{G}}{\partial z^2}=-2\mathrm{e}^{-\mathrm{i}\alpha\xi}\delta(y-\eta)\delta(z-\zeta). \tag{3.3}$$

Similar to (3.3), Fourier transform is applied to the boundary conditions in (2.4), (2.8) and (2.13), which provides

$$-\omega^2\tilde{G}+g\frac{\partial\tilde{G}}{\partial z}=0 \quad (|y|\leqslant b-0 \text{ and } z=0), \tag{3.4}$$

$$\left[L\left(\alpha^2-\frac{\partial^2}{\partial y^2}\right)^2+\rho_w g-m_i\omega^2\right]\frac{\partial\tilde{G}}{\partial z}-\rho_w\omega^2\tilde{G}=0 \quad (|y|\geqslant b+0 \text{ and } z=0), \tag{3.5}$$

and

$$\frac{\partial\tilde{G}}{\partial z}=0 \quad (z=-H). \tag{3.6}$$

In the channel with $|y|\leqslant b-0$, we may write $\tilde{G}$ in the vertical direction into the eigenfunction expansion as

$$\tilde{G}\equiv\tilde{G}_f=\sum_{m=0}^{\infty}\mathrm{e}^{-\mathrm{i}\alpha\xi}f_m(y)Z_m(z), \tag{3.7}$$

where the subscript f implies that the field point is in the water channel, and

$$Z_m(z)=\frac{\cosh[k_m(z+H)]}{\cosh(k_mH)}, \tag{3.8}$$

with k_m as the roots of the dispersion equation for a free surface, or

$$K_1(\omega,k)\equiv gk\tanh(kH)-\omega^2=0, \tag{3.9}$$

Here, k_0 is the purely positive real root and k_m ($m=1,\ldots,\infty$) are an infinite number of purely negative imaginary roots. It should be noted that the eigenfunction expansion of $\tilde{G}$ in (3.7) has already satisfied the boundary conditions in (3.4) and (3.6). Without loss of generality, we may assume that the source is in the channel or $|\eta|<b$. Substituting (3.7) into (3.3), we have

$$\sum_{m=0}^{\infty}Z_m(z)[f_m''(y)+\beta_m^2f_m(y)]=-2\delta(y-\eta)\delta(z-\zeta), \tag{3.10}$$

where $\beta_m^2=k_m^2-\alpha^2$, and the prime denotes derivative with respect to y. Using the orthogonality of the vertical mode $Z_m(z)$, we obtain

$$f_m''(y)+\beta_m^2f_m(y)=-\frac{2}{P_m}\delta(y-\eta)Z_m(\zeta), \tag{3.11}$$

where

$$\int_{-H}^{0} Z_m(z)Z_m(z)\,\mathrm{d}z = P_m, \tag{3.12}$$

with

$$P_m = \frac{2k_mH + \sinh(2k_mH)}{4k_m\cosh^2(k_mH)}. \tag{3.13}$$

A particular solution of (3.11) can be written as

$$f_m(y) = \frac{1}{\mathrm{i}\beta_m P_m}\exp(-\mathrm{i}\beta_m|y-\eta|)Z_m(\zeta). \tag{3.14}$$

Here, we have assumed $\mathrm{Im}(\beta_m) \leqslant 0$ when it is a complex number and $\beta_m > 0$ when it is a purely real number. Substituting (3.14) into (3.7), we can write the general solution as

$$\tilde{G}_f = \tilde{F} + \sum_{m=0}^{\infty}(a_m\Psi_m^a + b_m\Psi_m^b), \tag{3.15}$$

for $|y| \leqslant b-0$, where

$$\tilde{F} = \sum_{m=0}^{\infty}\frac{1}{\mathrm{i}\beta_m P_m}\exp(-\mathrm{i}\alpha\xi)\exp(-\mathrm{i}\beta_m|y-\eta|)Z_m(\zeta)Z_m(z), \tag{3.16}$$

and

$$\Psi_m^a = \exp(-\mathrm{i}\alpha\xi)\exp(-\mathrm{i}\beta_m(b-y))Z_m(z), \tag{3.17}$$

$$\Psi_m^b = \exp(-\mathrm{i}\alpha\xi)\exp(-\mathrm{i}\beta_m(b+y))Z_m(z). \tag{3.18}$$

The summation in (3.15) is the general solution of (3.3) when its right-hand side is zero. As shown in Appendix A, the first term on the right-hand side of (3.15) is in fact the Fourier transform of the Green function for full free surface without an ice sheet, which is the same as that in Wehausen & Laitone (1960).

In the ice covered waters, because $y \neq \eta$, equation (3.3) can be further written as

$$-\alpha^2\tilde{G} + \frac{\partial^2\tilde{G}}{\partial y^2} + \frac{\partial^2\tilde{G}}{\partial z^2} = 0. \tag{3.19}$$

Then by following the procedure in Li, Wu & Ren (2020*b*), we have

$$\tilde{G} \equiv \tilde{G}_{\pm} = \sum_{m=-2}^{\infty} c_m^{\pm}\Psi_m^{\pm}, \tag{3.20}$$

where the subscript $+$ and $-$ in $\tilde{G}$ are for $y \geqslant b+0$ and $y \leqslant -b-0$, respectively,

$$\Psi_m^{\pm} = \exp(-\mathrm{i}\alpha\xi)\exp(\mp\mathrm{i}\gamma_m(y\mp b))Q_m(z), \tag{3.21}$$

and

$$Q_m(z) = \frac{\cosh[\kappa_m(z+H)]}{\cosh(\kappa_m H)}, \tag{3.22}$$

with κ_m being the roots of the dispersion equation for ice sheet or

$$K_2(\omega,k) \equiv (Lk^4 + \rho_w g - m_i\omega^2)k\tanh(kH) - \rho_w\omega^2 = 0. \tag{3.23}$$

Here, κ_{-1} and κ_{-2} are two complex roots with negative imaginary parts and symmetric about the imaginary axis, κ_0 is the purely positive real root and κ_m $(m = 1,\ldots,\infty)$

are an infinite number of purely negative imaginary roots. In (3.21), $\gamma_m^2 = \kappa_m^2 - \alpha^2$ and $\mathrm{Im}(\gamma_m) \leqslant 0$ when it is a complex number and $\gamma_m > 0$ when it is a purely real number, which is based on the requirement of the radiation condition. It should be noted that $\tilde{G}$ in (3.20) has already satisfied the boundary conditions in (3.5) and (3.6).

There are four sets of unknown coefficients in (3.15) and (3.20), i.e. a_m, b_m, c_m^+ and c_m^-. These can be determined through the continuous conditions at the interfaces $y = \pm b$ or

$$\tilde{G}_\pm\Big|_{y=\pm b} = \tilde{G}_f\Big|_{y=\pm b}, \tag{3.24}$$

and

$$\frac{\partial \tilde{G}_\pm}{\partial y}\bigg|_{y=\pm b} = \frac{\partial \tilde{G}_f}{\partial y}\bigg|_{y=\pm b}, \tag{3.25}$$

together with the ice edge conditions. We may apply the Fourier transform (3.2) to the free ice edge conditions (2.9), which provides

$$\tilde{\mathcal{B}}\left(\frac{\partial \tilde{G}}{\partial z}\right) = 0 \quad \text{and} \quad \tilde{\mathcal{S}}\left(\frac{\partial \tilde{G}}{\partial z}\right) = 0, \tag{3.26a,b}$$

with

$$\tilde{\mathcal{B}} = \frac{\partial^2}{\partial y^2} - \nu\alpha^2, \tag{3.27}$$

$$\tilde{\mathcal{S}} = \frac{\partial}{\partial y}\left[\frac{\partial^2}{\partial y^2} - (2-\nu)\alpha^2\right]. \tag{3.28}$$

To impose these conditions, we may adopt Green's second theorem over the boundary Γ_+ of the domain with $y \geqslant b + 0$, which provides

$$\oint_{\Gamma_+}\left(\tilde{G}_+\frac{\partial \Psi_m^+}{\partial n} - \frac{\partial \tilde{G}_+}{\partial n}\Psi_m^+\right)\mathrm{d}l = 0. \tag{3.29}$$

Here, it should be noted that $\tilde{G}_+$ and Ψ_m^+ should satisfy the same boundary conditions on the flat seabed, ice sheet and the vertical surface at the far field $y = +\infty$. Removing the zero terms, we have

$$-\int_{-H}^{0}\left(\tilde{G}_+\frac{\partial \Psi_m^+}{\partial y} - \frac{\partial \tilde{G}_+}{\partial y}\Psi_m^+\right)_{y=+b}\mathrm{d}z + \int_{+b}^{+\infty}\left(\tilde{G}_+\frac{\partial \Psi_m^+}{\partial z} - \frac{\partial \tilde{G}_+}{\partial z}\Psi_m^+\right)_{z=0}\mathrm{d}y = 0. \tag{3.30}$$

Equation (3.5) provides

$$\tilde{G}_+ = \frac{L}{\rho_w\omega^2}\left(\alpha^4 - 2\alpha^2\frac{\partial^2}{\partial y^2} + \frac{\partial^4}{\partial y^4}\right)\frac{\partial \tilde{G}_+}{\partial z} + \frac{\rho_w g - m_i\omega^2}{\rho_w\omega^2}\frac{\partial \tilde{G}_+}{\partial z}, \tag{3.31}$$

which is also satisfied by ψ_m^+. Substituting (3.31) into (3.30), and using integration by parts over the ice sheet surface, we can obtain

$$\int_{-H}^{0}\left(\tilde{G}_+\frac{\partial\Psi_m^+}{\partial y}-\frac{\partial\tilde{G}_+}{\partial y}\Psi_m^+\right)_{y=+b}\mathrm{d}z+\frac{L}{\rho_w\omega^2}\left[2\alpha^2\left(\frac{\partial\tilde{G}_+}{\partial z}\frac{\partial^2\Psi_m^+}{\partial y\partial z}-\frac{\partial^2\tilde{G}_+}{\partial y\partial z}\frac{\partial\Psi_m^+}{\partial z}\right)\right.$$
$$\left.+\left(\frac{\partial^4\tilde{G}_+}{\partial y^3\partial z}\frac{\partial\Psi_m^+}{\partial z}-\frac{\partial\tilde{G}_+}{\partial z}\frac{\partial^4\Psi_m^+}{\partial y^3\partial z}\right)-\left(\frac{\partial^3\tilde{G}_+}{\partial y^2\partial z}\frac{\partial^2\Psi_m^+}{\partial y\partial z}-\frac{\partial^2\tilde{G}_+}{\partial y\partial z}\frac{\partial^3\Psi_m^+}{\partial y^2\partial z}\right)\right]_{y=+b,z=0}=0. \tag{3.32}$$

Similarly, we have at $y=-b$

$$\int_{-H}^{0}\left(\tilde{G}_-\frac{\partial\Psi_m^-}{\partial y}-\frac{\partial\tilde{G}_-}{\partial y}\Psi_m^-\right)_{y=-b}\mathrm{d}z+\frac{L}{\rho_w\omega^2}\left[2\alpha^2\left(\frac{\partial\tilde{G}_-}{\partial z}\frac{\partial^2\Psi_m^-}{\partial y\partial z}-\frac{\partial^2\tilde{G}_-}{\partial y\partial z}\frac{\partial\Psi_m^-}{\partial z}\right)\right.$$
$$\left.+\left(\frac{\partial^4\tilde{G}_-}{\partial y^3\partial z}\frac{\partial\Psi_m^-}{\partial z}-\frac{\partial\tilde{G}_-}{\partial z}\frac{\partial^4\Psi_m^-}{\partial y^3\partial z}\right)-\left(\frac{\partial^3\tilde{G}_-}{\partial y^2\partial z}\frac{\partial^2\Psi_m^-}{\partial y\partial z}-\frac{\partial^2\tilde{G}_-}{\partial y\partial z}\frac{\partial^3\Psi_m^-}{\partial y^2\partial z}\right)\right]_{y=-b,z=0}=0. \tag{3.33}$$

Invoking the free ice edge condition (3.26*a*,*b*), we have

$$\frac{\partial^3\tilde{G}_\pm}{\partial y^2\partial z}=\nu\alpha^2\frac{\partial\tilde{G}_\pm}{\partial z}\quad\text{and}\quad\frac{\partial^4\tilde{G}_\pm}{\partial y^3\partial z}=(2-\nu)\alpha^2\frac{\partial^2\tilde{G}_\pm}{\partial y\partial z} \tag{3.34a,b}$$

at $y=\pm b$ and $z=0$. Substituting this equation into (3.32) and (3.33), we obtain

$$\int_{-H}^{0}\left(\tilde{G}_f\frac{\partial\Psi_m^\pm}{\partial y}-\frac{\partial\tilde{G}_\pm}{\partial y}\Psi_m^\pm\right)_{y=\pm b}\mathrm{d}z+\frac{L}{\rho_w\omega^2}\left\{\alpha^2\left[(2-\nu)\frac{\partial\tilde{G}_\pm}{\partial z}\frac{\partial^2\Psi_m^\pm}{\partial y\partial z}\right.\right.$$
$$\left.\left.-\nu\frac{\partial^2\tilde{G}_\pm}{\partial y\partial z}\frac{\partial\Psi_m^\pm}{\partial z}\right]+\frac{\partial^2\tilde{G}_\pm}{\partial y\partial z}\frac{\partial^3\Psi_m^\pm}{\partial y^2\partial z}-\frac{\partial\tilde{G}_\pm}{\partial z}\frac{\partial^4\Psi_m^\pm}{\partial y^3\partial z}\right\}_{y=\pm b,z=0}=0, \tag{3.35}$$

where the continuity condition (3.24) has been used. It should be noted that the free ice edge condition has been imposed in (3.35) through replacing the corresponding terms on the ice edge in (3.32) and (3.33). There is no need to have further actions to impose this condition. The way to satisfy the ice edge condition here is similar to that of Ren *et al.* (2016). To impose the continuity condition (3.25), we multiply both sides of (3.15) with $Z_m(z)$ and then integrate with respect to z. This gives

$$\begin{aligned}\int_{-H}^{0}\frac{\partial\tilde{G}_+}{\partial y}Z_m(z)\,\mathrm{d}z&=\int_{-H}^{0}\frac{\partial\tilde{G}_f}{\partial y}Z_m(z)\,\mathrm{d}z\\&=\mathrm{i}\beta_mP_m(a_m-b_m\exp(-2\mathrm{i}\beta_mb))\\&\quad-\exp(-\mathrm{i}\alpha\xi)\exp(-\mathrm{i}\beta_m(b-\eta))Z_m(\zeta),\end{aligned} \tag{3.36}$$

$$\begin{aligned}\int_{-H}^{0}\frac{\partial\tilde{G}_-}{\partial y}Z_m(z)\,\mathrm{d}z&=\int_{-H}^{0}\frac{\partial\tilde{G}_f}{\partial y}Z_m(z)\,\mathrm{d}z\\&=\mathrm{i}\beta_mP_m(a_m\exp(-2\mathrm{i}\beta_mb)-b_m)\\&\quad+\exp(-\mathrm{i}\alpha\xi)\exp(-\mathrm{i}\beta_m(b+\eta))Z_m(\zeta),\end{aligned} \tag{3.37}$$

for $y = +b$ and $y = -b$, respectively, in which (3.12) has been used. Substituting (3.15) and (3.20) into (3.35) and (3.36), we have at $y = +b$

$$\gamma_m \sum_{\tilde{m}=0}^{\infty} (a_{\tilde{m}} + b_{\tilde{m}} \exp(-2\mathrm{i}\beta_{\tilde{m}} b)) V_{m,\tilde{m}} - c_m^+ \gamma_m U_m - \frac{LT_m}{\rho_w \omega^2} \sum_{\tilde{m}=-2}^{\infty} c_{\tilde{m}}^+ T_{\tilde{m}} [\nu\alpha^2 (\gamma_{\tilde{m}} + \gamma_m) - 2\alpha^2 \gamma_m + \gamma_m^2 (\gamma_{\tilde{m}} - \gamma_m) - \gamma_{\tilde{m}} (\kappa_m^2 + \kappa_{\tilde{m}}^2)] = \mathrm{i}\gamma_m \sum_{\tilde{m}=0}^{\infty} \frac{1}{\beta_{\tilde{m}} P_{\tilde{m}}} \exp(-\mathrm{i}\beta_{\tilde{m}} (b - \eta)) Z_{\tilde{m}}(\zeta) V_{m,\tilde{m}}, \tag{3.38}$$

$$\beta_m P_m (b_m \exp(-2\mathrm{i}\beta_m b) - a_m) - \sum_{\tilde{m}=-2}^{\infty} c_{\tilde{m}}^+ \gamma_{\tilde{m}} V_{\tilde{m},m} = \mathrm{i} \exp(-\mathrm{i}\beta_m (b - \eta)) Z_m(\zeta), \tag{3.39}$$

where

$$T_m = \kappa_m \tanh(\kappa_m H), \tag{3.40}$$

$$U_m = \frac{2\kappa_m H + \sinh(2\kappa_m H)}{4\kappa_m \cosh^2(\kappa_m H)} + \frac{2LT_m^2 \kappa_m^2}{\rho_w \omega^2}, \tag{3.41}$$

$$V_{m,\tilde{m}} = \int_{-H}^{0} Q_m Z_{\tilde{m}} \, \mathrm{d}z = \frac{T_m - k_{\tilde{m}} \tanh(k_{\tilde{m}} H)}{\kappa_m^2 - k_{\tilde{m}}^2}. \tag{3.42}$$

It should be noted that in (3.38) the following relationship has been used

$$\int_{-H}^{0} Q_m Q_{\tilde{m}} \, \mathrm{d}z = \delta_{m,\tilde{m}} U_m - \frac{LT_m T_{\tilde{m}}}{\rho_w \omega^2} (\kappa_m^2 + \kappa_{\tilde{m}}^2), \tag{3.43}$$

where $\delta_{m,\tilde{m}}$ is the Kronecker delta function. Similarly, we have at $y = -b$

$$\gamma_m \sum_{\tilde{m}=0}^{\infty} (a_{\tilde{m}} \exp(-2\mathrm{i}\beta_{\tilde{m}} b) + b_{\tilde{m}}) V_{m,\tilde{m}} - c_m^- \gamma_m U_m - \frac{LT_m}{\rho_w \omega^2} \sum_{\tilde{m}=-2}^{\infty} c_{\tilde{m}}^- T_{\tilde{m}} [\nu\alpha^2 (\gamma_{\tilde{m}} + \gamma_m) - 2\alpha^2 \gamma_m + \gamma_m^2 (\gamma_{\tilde{m}} - \gamma_m) - \gamma_{\tilde{m}} (\kappa_m^2 + \kappa_{\tilde{m}}^2)] = \mathrm{i}\gamma_m \sum_{\tilde{m}=0}^{\infty} \frac{1}{\beta_{\tilde{m}} P_{\tilde{m}}} \exp(-\mathrm{i}\beta_{\tilde{m}} (b + \eta)) Z_{\tilde{m}}(\zeta) V_{m,\tilde{m}}, \tag{3.44}$$

$$\beta_m P_m (a_m \exp(-2\mathrm{i}\beta_m b) - b_m) - \sum_{\tilde{m}=-2}^{\infty} c_{\tilde{m}}^- \gamma_{\tilde{m}} V_{\tilde{m},m} = \mathrm{i} \exp(-\mathrm{i}\beta_m (b + \eta)) Z_m(\zeta). \tag{3.45}$$

From (3.39) and (3.45), we can obtain

$$a_m = \frac{1}{\beta_m P_m(\exp(-4\mathrm{i}\beta_m b)-1)} \sum_{\tilde{m}=-2}^{\infty} (c_{\tilde{m}}^{+} + c_{\tilde{m}}^{-} \exp(-2\mathrm{i}\beta_m b))\gamma_{\tilde{m}} V_{\tilde{m},m} + \mathrm{i}Z_m(\zeta) \frac{\exp(-\mathrm{i}\beta_m(3b+\eta)) + \exp(-\mathrm{i}\beta_m(b-\eta))}{\beta_m P_m(\exp(-4\mathrm{i}\beta_m b)-1)}, \tag{3.46}$$

$$b_m = \frac{1}{\beta_m P_m(\exp(-4\mathrm{i}\beta_m b)-1)} \sum_{\tilde{m}=-2}^{\infty} (c_{\tilde{m}}^{+} \exp(-2\mathrm{i}\beta_m b) + c_{\tilde{m}}^{-})\gamma_{\tilde{m}} V_{\tilde{m},m} + \mathrm{i}Z_m(\zeta) \frac{\exp(-\mathrm{i}\beta_m(b+\eta)) + \exp(-\mathrm{i}\beta_m(3b-\eta))}{\beta_m P_m(\exp(-4\mathrm{i}\beta_m b)-1)}. \tag{3.47}$$

Substituting these two equations into (3.38), we have

$$\begin{aligned} &-c_m^{+}\gamma_m U_m + \gamma_m \sum_{\tilde{m}=0}^{\infty} \frac{V_{m,\tilde{m}}}{\beta_{\tilde{m}} P_{\tilde{m}}(\exp(-4\mathrm{i}\beta_{\tilde{m}} b)-1)} \\ &\quad \times \sum_{n=-2}^{\infty} [c_n^{+}(1+\exp(-4\mathrm{i}\beta_{\tilde{m}} b)) + 2c_n^{-}\exp(-2\mathrm{i}\beta_{\tilde{m}} b)]\gamma_n V_{n,\tilde{m}} \\ &\quad - \frac{LT_m}{\rho_w \omega^2} \sum_{\tilde{m}=-2}^{\infty} c_{\tilde{m}}^{+} T_{\tilde{m}} [\nu\alpha^2(\gamma_{\tilde{m}}+\gamma_m) - 2\alpha^2\gamma_m + \gamma_m^2(\gamma_{\tilde{m}}-\gamma_m) - \gamma_{\tilde{m}}(\kappa_m^2 + \kappa_{\tilde{m}}^2)] \\ &= -2\mathrm{i}\gamma_m \sum_{\tilde{m}=0}^{\infty} \frac{\exp(-\mathrm{i}\beta_{\tilde{m}}(b-\eta)) + \exp(-\mathrm{i}\beta_{\tilde{m}}(3b+\eta))}{\beta_{\tilde{m}} P_{\tilde{m}}(\exp(-4\mathrm{i}\beta_{\tilde{m}} b)-1)} Z_{\tilde{m}}(\zeta) V_{m,\tilde{m}}. \end{aligned} \tag{3.48}$$

Similarly, we have for (3.44)

$$\begin{aligned} &-c_m^{-}\gamma_m U_m + \gamma_m \sum_{\tilde{m}=0}^{\infty} \frac{V_{m,\tilde{m}}}{\beta_{\tilde{m}} P_{\tilde{m}}(\exp(-4\mathrm{i}\beta_{\tilde{m}} b)-1)} \\ &\quad \times \sum_{n=-2}^{\infty} [2c_n^{+}\exp(-2\mathrm{i}\beta_{\tilde{m}} b) + c_n^{-}(1+\exp(-4\mathrm{i}\beta_{\tilde{m}} b))]\gamma_n V_{n,\tilde{m}} \\ &\quad - \frac{LT_m}{\rho_w \omega^2} \sum_{\tilde{m}=-2}^{\infty} c_{\tilde{m}}^{-} T_{\tilde{m}} [\nu\alpha^2(\gamma_{\tilde{m}}+\gamma_m) - 2\alpha^2\gamma_m + \gamma_m^2(\gamma_{\tilde{m}}-\gamma_m) - \gamma_{\tilde{m}}(\kappa_m^2 + \kappa_{\tilde{m}}^2)] \\ &= -2\mathrm{i}\gamma_m \sum_{\tilde{m}=0}^{\infty} \frac{\exp(-\mathrm{i}\beta_{\tilde{m}}(b+\eta)) + \exp(-\mathrm{i}\beta_{\tilde{m}}(3b-\eta))}{\beta_{\tilde{m}} P_{\tilde{m}}(\exp(-4\mathrm{i}\beta_{\tilde{m}} b)-1)} Z_{\tilde{m}}(\zeta) V_{m,\tilde{m}}. \end{aligned} \tag{3.49}$$

This shows c_m^{+} and c_m^{-} can be solved first independently from (3.48) and (3.49), after which a_m and b_m can be obtained directly from (3.46) and (3.47).

In practical computations, (3.48) and (3.49) can be solved through truncating the infinite summation at a finite number $m = M$. Here, it should be noted that the matrix coefficients for the unknowns only depend on the value of α and are independent of the source position. Therefore, the inverse does not have to be recalculated at different source position.

In addition, from (3.46) and (3.47), we can see that the truncation for a_m and b_m can be made at a value different from M.

The Green function G can be found through applying the inverse Fourier transform to $\tilde{G}$, or

$$G = \int_{-\infty}^{+\infty} \tilde{G}\, \mathrm{e}^{+\mathrm{i}\alpha x}\, \mathrm{d}\alpha. \tag{3.50}$$

Substituting (3.15) and (3.20) into this equation, and using the symmetry property of $\tilde{G}$, we have

$$G = \begin{cases} 2\displaystyle\sum_{m=-2}^{\infty} Q_m(z) \int_0^{+\infty} c_m^{+} \exp(-\mathrm{i}\gamma_m(y-b)) \cos[\alpha(x-\xi)]\, \mathrm{d}\alpha, & y \geqslant b+0 \\ F + 2\displaystyle\sum_{m=0}^{\infty} Z_m(z) \int_0^{+\infty} (a_m \exp(-\mathrm{i}\beta_m(b-y)) \\ \quad + b_m \exp(-\mathrm{i}\beta_m(b+y))) \cos[\alpha(x-\xi)]\, \mathrm{d}\alpha, & |y| \leqslant b-0 \\ 2\displaystyle\sum_{m=-2}^{\infty} Q_m(z) \int_0^{+\infty} c_m^{-} \exp(+\mathrm{i}\gamma_m(y+b)) \cos[\alpha(x-\xi)]\, \mathrm{d}\alpha, & y \leqslant -b-0. \end{cases} \tag{3.51}$$

where

$$F = \sum_{m=0}^{\infty} \frac{1}{\mathrm{i}P_m} Z_m(\zeta) Z_m(z) I_m, \tag{3.52}$$

with

$$I_m = \int_{-\infty}^{+\infty} \frac{1}{\beta_m} \exp(+\mathrm{i}\alpha(x-\xi)) \exp(-\mathrm{i}\beta_m|y-\eta|)\, \mathrm{d}\alpha = \pi H_0^{(2)}(k_m R). \tag{3.53}$$

Here, F is identical to the Green function for a free surface in (A16), and (A11) and (A14) have been used in (3.53). It should be noted that when the ice thickness $h = 0$, the Green function in (3.51) will become that for a free surface, as shown in Appendix A. As shown in Appendix B, we also have that the Green function is symmetric regarding the source and field points or

$$G(p, q) - G(q, p) = 0. \tag{3.54}$$

When $\alpha \to k_0$ or $\beta_0^2 = k_0^2 - \alpha^2 \to 0$, (3.38) and (3.44) show that there is a singularity on the right-hand side. However, it is of square root order, or $1/(k_0^2 - \alpha^2)^{1/2}$ in the inverse Fourier transform, which numerically can be computed through the Gauss–Chebyshev procedure (Abramowitz & Stegun 1965). Special care should be paid to the integrals over the domain $\kappa_0 < \alpha < k_0$ when $k_0 > \kappa_0$. In such a case, there are non-decaying wave modes at $x = \pm\infty$ at discrete wave numbers of $\kappa_0 < \alpha_1 < \ldots < \alpha_N < k_0$, which correspond to the trapped modes in Porter (2018). This means that there may be a number of poles at α_j $(j = 1, \ldots, N)$ of the integrand in (3.51). To satisfy the radiation condition, which states that the waves should propagate away from the source, the integral route in (3.51) from 0 to $+\infty$ should pass over these poles. Then, through applying the Fourier integrals in Wehausen & Laitone (1960), we can obtain the asymptotic expression of (3.51) at

$|x-\xi| \to +\infty$, or

$$G_\infty \equiv \lim_{|x-\xi|\to+\infty} G = -2\mathrm{i}\pi \sum_{j=1}^{N} \exp(-\mathrm{i}\alpha_j|x-\xi|) \times \begin{cases} \displaystyle\sum_{m=-2}^{\infty} Q_m(z) \lim_{\alpha\to\alpha_j} [(\alpha-\alpha_j)c_m^+ \exp(-\mathrm{i}\gamma_{m,j}(y-b))], & y \geqslant b+0 \\ \displaystyle\sum_{m=0}^{\infty} Z_m(z) \lim_{\alpha\to\alpha_j} \{(\alpha-\alpha_j)[a_m \exp(-\mathrm{i}\beta_{m,j}(b-y)) \\ \quad +b_m \exp(-\mathrm{i}\beta_{m,j}(b+y))]\}, & |y| \leqslant b-0 \\ \displaystyle\sum_{m=-2}^{\infty} Q_m(z) \lim_{\alpha\to\alpha_j} [(\alpha-\alpha_j)c_m^- \exp(+\mathrm{i}\gamma_{m,j}(y+b))], & y \leqslant -b-0. \end{cases} \tag{3.55}$$

For $|y| \leqslant b-0$, the wave component of α_j exists inside the channel. However, for $|y| \geqslant b+0$ below the ice sheet, $\gamma_{m,j}$, corresponding to α_j, always have $\mathrm{Im}(\gamma_{m,j}) < 0$, which indicates that the wave of α_j will decay exponentially with y. It should also be noted that F in (3.51) for $|y| \leqslant b-0$ corresponds to the cylindrical wave at the far field, the amplitude of which decreases with $1/\sqrt{R}$. Therefore, this term has been dropped in (3.55) because it will diminish as $|x-\xi| \to +\infty$.

To search for α_j numerically, we may use the fact that the singularities of a_m, b_m, c_m^+ and c_m^- are of the form of $1/(\alpha-\alpha_j)$. When (3.46)– (3.49) are solved at different α, sufficiently small step $\Delta\alpha$ is used. When the results become very large at both α and $\alpha+\Delta\alpha$, and their signs are different, one of the α_j will exist within this step. The accuracy of α_j can be refined by using the further smaller steps within the region.

The calculation of the limit in (3.55) needs some special attention. In theory, the limit can be obtained through L'Hospital's rule. However, the integrand and its singularities here are not explicitly given and they are obtained from the numerical procedure described previously. Thus, the following method is used to calculate the limit. We may consider a function $f(\alpha)$, which has a singularity in the form $f(\alpha) \to g(\alpha)/(\alpha-\alpha_j)$ as $\alpha \to \alpha_j$. Then, $g(\alpha_j) = \lim_{\alpha\to\alpha_j}(\alpha-\alpha_j)f(\alpha)$ can be found numerically by

$$\begin{aligned} g(\alpha_j) &= \frac{g(\alpha_j+\Delta\alpha)+g(\alpha_j-\Delta\alpha)}{2} + O[g''(\alpha_j)(\Delta\alpha)^2] \\ &\approx \Delta\alpha \frac{f(\alpha_j+\Delta\alpha)-f(\alpha_j-\Delta\alpha)}{2}. \end{aligned} \tag{3.56}$$

3.2. *Solution to the disturbed velocity potential for a body in the ice channel*

As shown in Appendix B, we have the boundary integral equation for the disturbed velocity potential ϕ as follow

$$\ell\phi(p) = \int_{S_B} \left[G(p,q)\frac{\partial\phi(q)}{\partial n_q} - \frac{\partial G(p,q)}{\partial n_q}\phi(q) \right] \mathrm{d}s_q, \tag{3.57}$$

where only the integral over the mean wetted body surface S_B is needed, and ℓ is the solid angle at point p. As noted by Lee, Newman & Zhu (1996) in the free surface problem, for floating bodies there could exist a discrete spectrum of irregular frequencies, at which

the solution to the boundary integral equation is non-unique. Similar irregular frequencies also exist in (3.57). To remove the irregular frequencies, we follow the procedure described in Lee *et al.* (1996) and rewrite (3.57) equivalently as

$$\ell\phi(p) + \int_{S_B+S_E} \frac{\partial G(p,q)}{\partial n_q}\phi(q)\,\mathrm{d}s_q = \int_{S_B} G(p,q)\frac{\partial \phi(q)}{\partial n_q}\,\mathrm{d}s_q \quad \text{for } p \in S_B, \tag{3.58}$$

and

$$-4\pi\phi(p) + \int_{S_B+S_E} \frac{\partial G(p,q)}{\partial n_q}\phi(q)\,\mathrm{d}s_q = \int_{S_B} G(p,q)\frac{\partial \phi(q)}{\partial n_q}\,\mathrm{d}s_q \quad \text{for } p \in S_E, \tag{3.59}$$

where S_E is the extended surface interior the body at $z = 0$. This has been found to remove the irregular frequencies effectively.

For the radiation problem, $\phi = \phi_j$ and $\partial\phi_j/\partial n = n_j$ can be used directly in the integral equations (3.58) and (3.59). However, for the diffraction problem, it has two components. The incident wave will be diffracted by both the channel and the body. Thus, similar to Li *et al.* (2018*b*), we write the total diffracted potential as

$$\phi_D = \phi_D^1 + \phi_D^2, \tag{3.60}$$

where ϕ_D^1 is the diffracted potential of the flexural gravity incident potential ϕ_I by the water channel, and ϕ_D^2 is that by the body to $\varphi = \phi_I + \phi_D^1$. It should be mentioned that φ satisfies the ice edge condition (2.9). Here, the incident potential ϕ_I can be written as

$$\phi_I = \varphi_I(y,z)\,\mathrm{e}^{-\mathrm{i}\kappa_x x}, \tag{3.61}$$

with

$$\varphi_I = A\,\mathrm{e}^{-\mathrm{i}\kappa_y y}Q_0(z), \tag{3.62}$$

where $A = \mathrm{i}\omega/[\kappa_0\tanh(\kappa_0 H)]$, $\kappa_x = \kappa_0\cos\beta$ and $\kappa_y = \kappa_0\sin\beta$. Correspondingly, the potential φ can be written as

$$\varphi = \bar{\varphi}(y,z)\,\mathrm{e}^{-\mathrm{i}\kappa_x x}. \tag{3.63}$$

Here $\bar{\varphi}$ or ϕ_D^1 can be obtained virtually in the same way as $\tilde{G}$. The main difference is that α should be replaced by κ_x and terms on the right-hand sides due to $\tilde{F}$ in (3.46)–(3.49) should be replaced by the contribution due to ϕ_I. Because $\varphi = \phi_I + \phi_D^1$ satisfies the conditions at the ice sheet edge, then ϕ_D^2 should also satisfy these conditions. Thus, we can apply the integral equation (3.57) to ϕ_D^2 by imposing the boundary condition $\partial\phi_D^2/\partial n = -\partial\varphi/\partial n$ on the body surface.

After the velocity potentials have been found, the pressure at any point in fluid can be computed through the linearized Bernoulli equation. Then the hydrodynamic forces on the body can be obtained through integrating the pressure over its surface. Based on the decomposition of the velocity potential in (2.1), we may divide the total hydrodynamic loads into two parts, i.e. the radiation force due to the forced oscillatory motions and the wave exciting force due to the scattering potential (Newman 1977). For the radiation

potential, we have

$$\mu_{jk} - \mathrm{i}\frac{\lambda_{jk}}{\omega} = \rho_w \int_{S_B} \phi_k n_j \,\mathrm{d}s, \tag{3.64}$$

where μ_{jk} and λ_{jk} are the added mass and damping coefficient, respectively. For the scattering potential, we have

$$f_{E,j} = -\mathrm{i}\omega\rho_w \int_{S_B} \phi_0 n_j \,\mathrm{d}s, \tag{3.65}$$

where $f_{E,j}$ is the wave exciting force.

4. Numerical results

To provide meaningful results in physics, the typical values of the parameters of ice sheet and fluid are taken to be

$$\left.\begin{gathered} E = 5\ \text{GPa}, \quad \nu = 0.3, \quad \rho_i = 922.5\ \text{kg m}^{-3}, \quad h = 1\ \text{m}, \quad \rho_w = 1025\ \text{kg m}^{-3}, \\ H = 100\ \text{m}, \end{gathered}\right\} \tag{4.1}$$

which are similar to those obtained from the field experiment in polar regions (Squire *et al.* 1995). The channel width is chosen as $60\ \text{m} \leqslant 2b \leqslant 100\ \text{m}$, which can be developed, for example, by an icebreaker with azimuth thrusters (Riska, Lohi & Eronen 2005). In the following text, all the numerical results will be provided in the dimensionless form, based on the combinations of three basic parameters, i.e. density of water ρ_w, acceleration due to gravity $g = 9.8\ \text{m s}^{-2}$ and a characteristic length scale. For each case, the wave number k_0 for free surface wave is given, and the corresponding wave frequency ω can be obtained through the dispersion equation (3.9).

4.1. *Wave induced by a source submerged in the ice channel*

We first consider the wave induced by a source submerged in the channel confined by two semi-infinite ice sheets, with the ice sheet thickness $h = 1$ m taken as the characteristic length scale and the half channel width fixed to be $b = 50$ m. This is to shed some lights on some features of the free surface and the ice sheet deflection pattern. Numerical calculations are carried out through truncating the infinite summations in (3.51) to a finite number, or keeping only the first $M_G + 1$ terms. The wave elevation is computed based on the kinematic boundary condition, which gives

$$w = \frac{1}{\mathrm{i}\omega}\left.\frac{\partial G}{\partial z}\right|_{z=0}. \tag{4.2}$$

The values of α_j are obtained through the procedure described towards the end of § 3.1. It should be noted that α_j do not depend on the location of the source. However, each α_j corresponds to a wave in the channel either symmetric or antisymmetric about $y = 0$ (Porter 2018). When the source is located at the centre of the channel, only symmetric waves will be triggered. Thus, to capture all α_j, corresponding to both symmetric and antisymmetric modes, they are computed through the case with the source located at $(0, b/2, -H/100)$. To ensure the accuracy of α_j, as well as the accuracies of integration and the approximation of (3.56), the step $\Delta\alpha$ is chosen from the lowest value among 0.0001, $(\alpha_j - \alpha_{j-1})/50$ and $(\alpha_{j+1} - \alpha_j)/50$ when α is between α_{j-1} and α_{j+1}, where

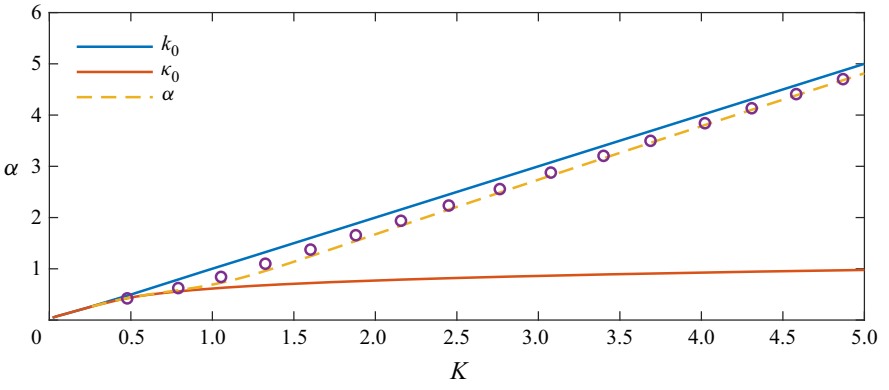

Figure 2. The first symmetric trapped mode α at a large water depth $H/h = 100$ against $K = \omega^2/g$. Open circles: α taken from figure 3 of Porter (2018) for infinite water depth. (The parameters of ice sheet and fluid as well as the characteristic length scale are taken to be the same as those in Porter 2018).

$\alpha_0 = \kappa_0$ for $j = 1$ and $\alpha_{N+1} = k_0$ for $j = N$ with N as the number of the singularities. Searching for α_j is done numerically through the Gauss elimination with partial pivoting for the matrix equation. When the solution of the unknown in the last line jumps from a large positive (negative) number $\mathcal{R}$ to a large negative (position) number $-\mathcal{R}$ within a small $\Delta\alpha$, it is assumed that α_j is within $\Delta\alpha$. Here we have used $\mathcal{R} = 10^{10}$ and $\Delta\alpha = 10^{-16}$. Figure 2 provides the first symmetric trapped mode α at a large water depth $H/h = 100$ against $K = \omega^2/g$. The infinite summations are truncated at $M_G = 100$. As a comparison, the result in Porter (2018) for infinite water depth is also provided, and the same parameters of ice sheet and fluid as well as the characteristic length scale are taken. It can be observed from this figure that the values of α for $H/h = 100$ are close to the values in Porter (2018) for infinite water depth. It should be noted that in the present formulation, the expansion in the vertical direction is, in fact, a cosine series. When H is very large, the terms required in the expansion to ensure convergence will increase rapidly. In particular, the series expansion cannot be used when $H = +\infty$. Instead, an integral form should be used to replace the series, similar to that Fourier series should be replaced by Fourier transform. Thus, the present work cannot be used for $H = +\infty$ directly. In fact, when H is very large, the series expansion will require a very large number of terms to ensure accuracy and the method become very inefficient. Therefore, larger water depth is not attempted. A more efficient method in such a case would be to use the integral form in the vertical direction, for example as in Li *et al.* (2018*b*).

Figure 3 shows the wave elevation w induced by a source with position $(\xi, \eta, \zeta) = (0, 0, -1)$ and wave number $k_0 = 0.1$ (the corresponding dimensional wave radian frequency ω is 0.99 rad s^{-1}). It can be observed from the figure that there is no visible difference between the results obtained by $M_G = 50$ and $M_G = 100$, indicating that the convergence has been achieved, and the former will be used for numerical computations of the Green function in this and following sections if it is not specifically specified.

In figure 4, the transverse variation of w with y at four different x are given, with the wave number being the same as that in figure 3. Two source positions are considered, namely $(\xi, \eta, \zeta) = (0, 0, -1)$ and $(\xi, \eta, \zeta) = (0, 25, -1)$. For $x/b = 30$, the wave elevation w_∞ computed by the asymptotic formula (3.55) is also provided, and the result agrees well with that obtained by the exact formula (4.2) for both central and non-central source positions. From figure 4, it can be seen that w is generally discontinuous at the ice edge between free

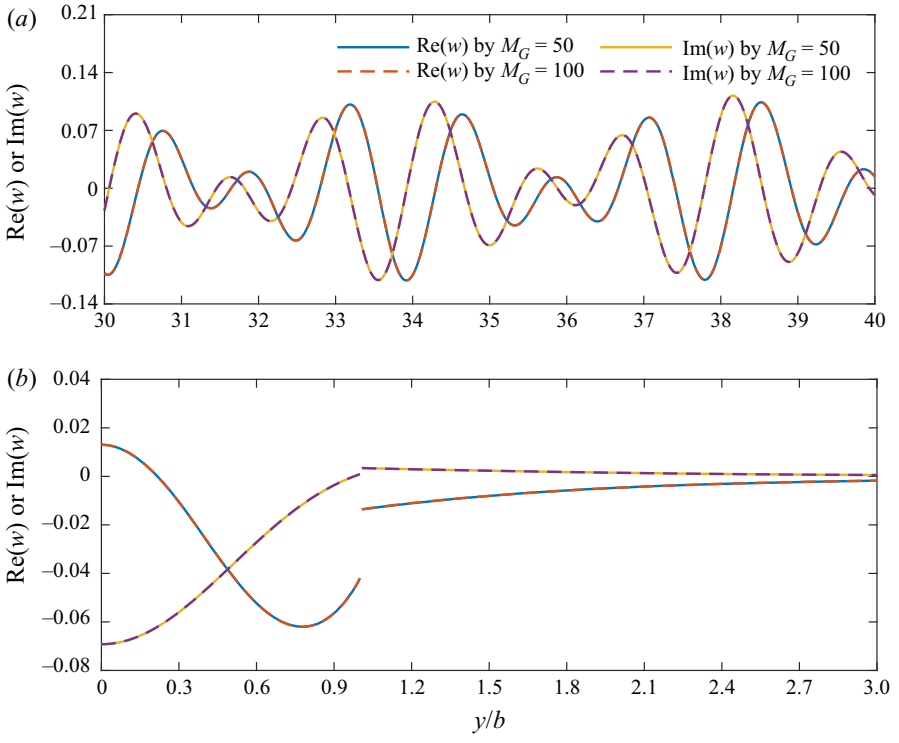

Figure 3. The real part (Re) and imaginary part (Im) of wave elevation w induced by a source at $(\xi, \eta, \zeta) = (0, 0, -1)$: (*a*) w varies along the longitudinal cut with $y/b = 0$; (*b*) w varies along the transverse cut with $x/b = 35$ ($k_0 = 0.1$, $b = 50$, $h = 1$ m is taken as the characteristic length scale).

surface and ice sheet. This is because that although the kinematic boundary conditions on free surface and ice sheet are the same, their dynamic boundary conditions are different.

The discontinuity of w across the ice sheet edge can be observed more clearly from w at $y/b = 1 - 0$ and $y/b = 1 + 0$ in figure 5, which shows the wave elevation w_∞ along the longitudinal cut at different y computed by the asymptotic formula (3.55). It is well known that for full free surface problem (Wehausen & Laitone 1960) or ice sheet problem (Li, Wu & Shi 2018*c*), the Green function will decrease in the form of $1/\sqrt{R}$ with R as the horizontal distance between the field and source points. However, this is not the case for the problem of an open water channel confined by two semi-infinite ice sheets. From figure 5, it can be seen that at the far field when x changes, w will oscillate with periodical components both in the channel and in the ice sheet, and the wave numbers of the oscillation are $\alpha_1, \ldots, \alpha_N$. In (3.55), because $\kappa_0 < \alpha_j < k_0$ we have that all $\gamma_{m,j}$ will be complex with a negative imaginary part. This indicates that the wave components corresponding to the trapped wave modes α_j will decay exponentially with y away from the ice sheet edge. The decay can be seen from figure 5 for wave elevation w_∞ by the asymptotic formula along the longitudinal cut at different y, and more clearly observed from figure 6, which shows a contour plot of w_∞ as a function of x and y.

In figure 7, the wave elevation w along the longitudinal cut $y/b = 0$ at large x is shown for four different wave numbers, namely $k_0 = 0.1$, 0.2, 0.3 and 0.4 (the corresponding dimensional wave radian frequencies ω are 0.99, 1.40, 1.71 and 1.98 rad s^{-1}). The source point q is located at $(0, 0, -1)$, and w is computed by the asymptotic formula (3.55). The corresponding trapped modes α_j for each k_0 are provided in table 1 to four decimal places,

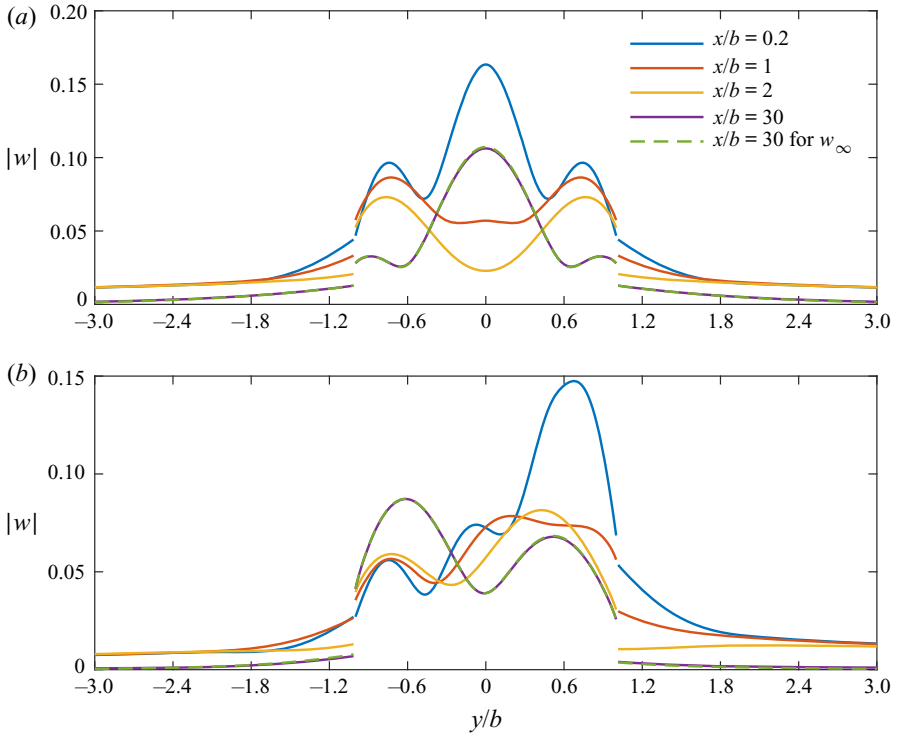

Figure 4. The modulus of wave elevation w induced by a source: (a) $(\xi, \eta, \zeta) = (0, 0, -1)$; (b) $(\xi, \eta, \zeta) = (0, 25, -1)$ ($k_0 = 0.1$, $b = 50$, $h = 1$ m is taken as the characteristic length scale).

together with the corresponding amplitude w_j. Because $\eta = 0$, only the symmetric modes are non-zero. It can be seen from table 1 that the number N of α_j increases with k_0. This leads to a more oscillatory w, as can be observed in figure 7. From table 1, it can be also observed that at larger k_0, when j is close to N, different α_j are close to each other and α_N is very close to k_0. In the numerical computation, it is noted that when $\alpha = \alpha_j \pm \Delta\alpha$, the magnitudes of a_m, b_m, c_m^+ and c_m^- are no longer exceedingly large when $\Delta\alpha = O(10^{-4})$. Here, $\alpha_{j+1} - \alpha_j = O(10^{-3})$, and α_{j+1} does not have a major effect on w_j.

The stress (strain) of the ice sheet is associated with its possible breakup when it becomes excessive. The principal strain ε can be obtained by the eigenvalues of the strain tensor matrix (Timoshenko & Woinowsky 1959)

$$\sigma = -\frac{h}{2}\begin{bmatrix} \dfrac{\partial^2 W}{\partial x^2} & \dfrac{\partial^2 W}{\partial x \partial y} \\ \dfrac{\partial^2 W}{\partial x \partial y} & \dfrac{\partial^2 W}{\partial y^2} \end{bmatrix}, \tag{4.3}$$

or the solution of $\det[\sigma - \varepsilon I] = 0$, which provides

$$\varepsilon_{1,2} = -\frac{h}{4}\left[\left(\frac{\partial^2 W}{\partial x^2} + \frac{\partial^2 W}{\partial y^2}\right) \pm \sqrt{\left(\frac{\partial^2 W}{\partial x^2} + \frac{\partial^2 W}{\partial y^2}\right)^2 + 4\left(\frac{\partial^2 W}{\partial x \partial y}\right)^2}\right]. \tag{4.4}$$

Invoking (4.2), the physical deflection of the ice sheet can be written as

$$W(x, y, t) = \mathrm{Re}(w)\cos(\omega t) - \mathrm{Im}(w)\sin(\omega t). \tag{4.5}$$

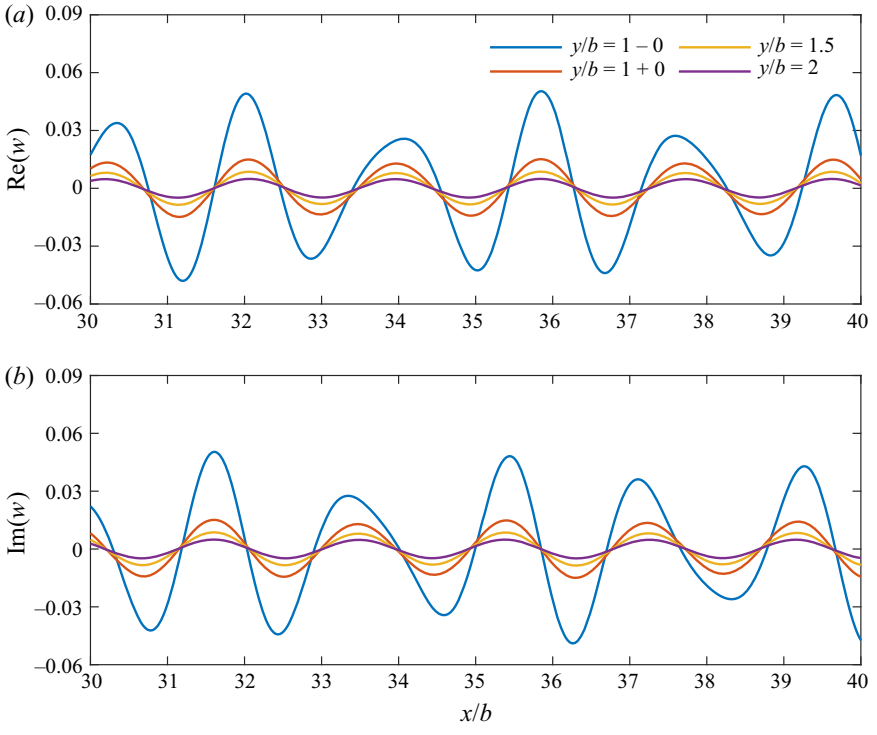

Figure 5. The wave elevation w induced by a source at $(\xi, \eta, \zeta) = (0, 0, -1)$: ($a$) real part (Re) of w_∞; (b) imaginary part (Im) of w_∞ ($k_0 = 0.1$, $b = 50$, $h = 1$ m is taken as the characteristic length scale).

Then, at each point in the ice sheet the maximum principal strain, can be found as the largest eigenvalue ε_M of σ in (4.3) as ωt varies from 0 to 2π. Figure 8 shows the maximum principal strain ε_M induced by a source with position $(\xi, \eta, \zeta) = (0, 0, -1)$. The wave numbers are taken to be the same as those in figure 7. From figure 8(a) which gives ε_M along the longitudinal cut with $y/b = 1 + 0$, we have that ε_M will increase to a maximum at a distance away from the source. When $|x - \xi|$ is very large or only the waves due to the trapped wave modes have contributions to ε_M, it can be expected from (3.55) that ε_M will oscillate with periodical components (wave numbers as $\alpha_1, \ldots, \alpha_N$) against $|x - \xi|$. When $x = \xi$ and y varies, it can be seen from figure 8 that ε_M will first decrease with y and it will then increase and reach its maximum rapidly. After the maximum ε_M it will decrease with y slowly. From (3.55), at each of these α_j modes G decays exponentially with y. However, at a finite $|x - \xi|$, in addition to these modes, there are also some local modes at which G decays in form of $1/\sqrt{|y|}$ which is similar to that in the case when water surface is fully covered by an ice sheet Li *et al.* (2018*c*).

4.2. *Wave interactions with a body floating on the ice channel*

We now consider the wave interactions with a body floating on the ice channel. The body used for this case study is a barge of length L_L, beam L_B and draught D. The half beam or $L_B/2 = 10$ m is chosen as the characteristic length scale. Computations are carried out for $L_L/L_B = 4$ and $D/L_B = 0.25$. These ratios are the same as those in Newman (2017) for the tank problem. The rotational centre (x_0, y_0, z_0) of the barge is taken at the geometry centre. Both the wave radiation and diffraction problems are solved, and the

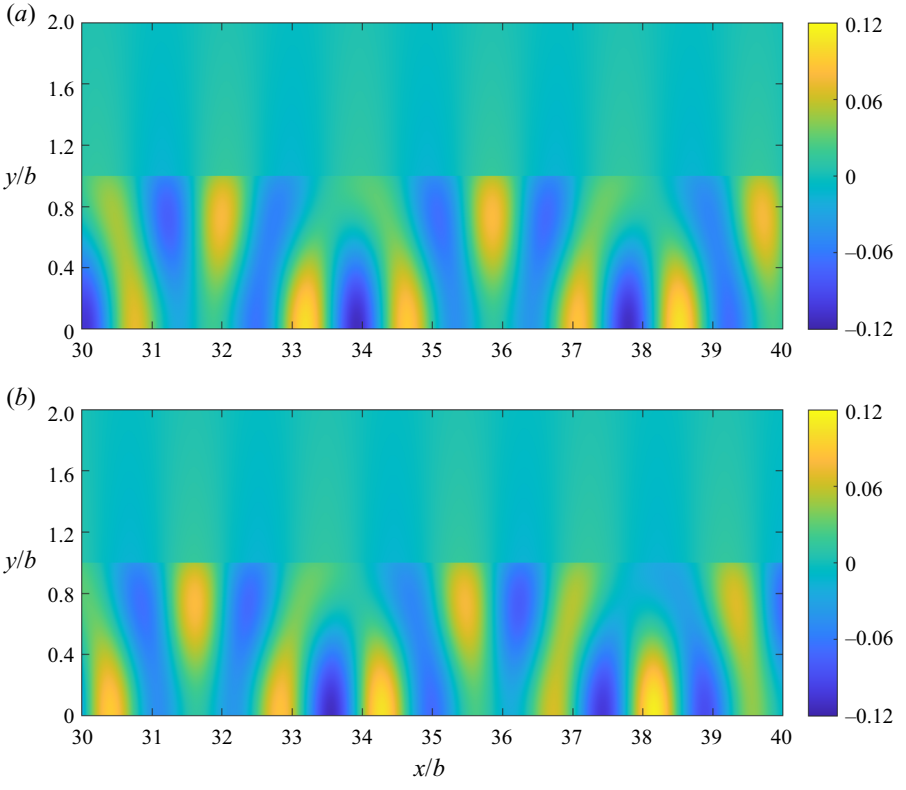

Figure 6. The (a) real part and (b) imaginary part of wave elevation w_∞ induced by a source at $(\xi, \eta, \zeta) = (0, 0, -1)$ ($k_0 = 0.1$, $b = 50$, $h = 1$ m is taken as the characteristic length scale).

incident flexural gravity wave is assumed to be from $\beta = \pi/4$. The barge is assumed to float at the centre of the channel or $y_0 = 0$. Two channel widths are considered, i.e. $b = 3$ and $b = 5$. To conduct numerical computations, the body surface S_B is discretized into $N_B = 1408$ flat panels, as shown in figure 9. The extended interior surface S_E introduced to remove the irregular frequencies is discretized into $N_E = 156$ flat panels. To obtain the diffracted potential ϕ_D^1 by the channel due to ϕ_I, the first $M_D + 1$ terms are kept in its eigenfunction expansion, and $M_D = 200$ is taken for calculation. It has been observed that further increase of N_B and N_E, M_D and M_G will give graphically indistinguishable results in the figures given here.

The diagonal terms of the added mass and damping coefficient for $b = 3$ with $y_0 = 0$ and for $b = 5$ with $y_0 = 0$ and $y_0 = 2$, are presented in figures 10 and 11 respectively against free surface wave number k_0, whereas the wave exciting forces are plotted in figure 12. The hydrodynamic forces for the barge in open sea are also provided. The wave number k_0 varies from 0.02 to 4, and the increment has been chosen to be 0.02 to capture the more detailed oscillatory features of the curves. When k_0 is small, it can be seen that the hydrodynamic forces in the ice channel case are all very close to those in the open sea case. When $k_0 \to 0$ or $\omega \to 0$, both the leading term of the boundary conditions on ice sheet and free surface will be $\partial\phi_j/\partial z = 0$. This indicates that as $k_0 \to 0$ the upper surface boundary condition for ice channel will tend to be the same as that for open sea. Thus the hydrodynamic forces for ice channel will be very similar to those for open sea when k_0 is small.

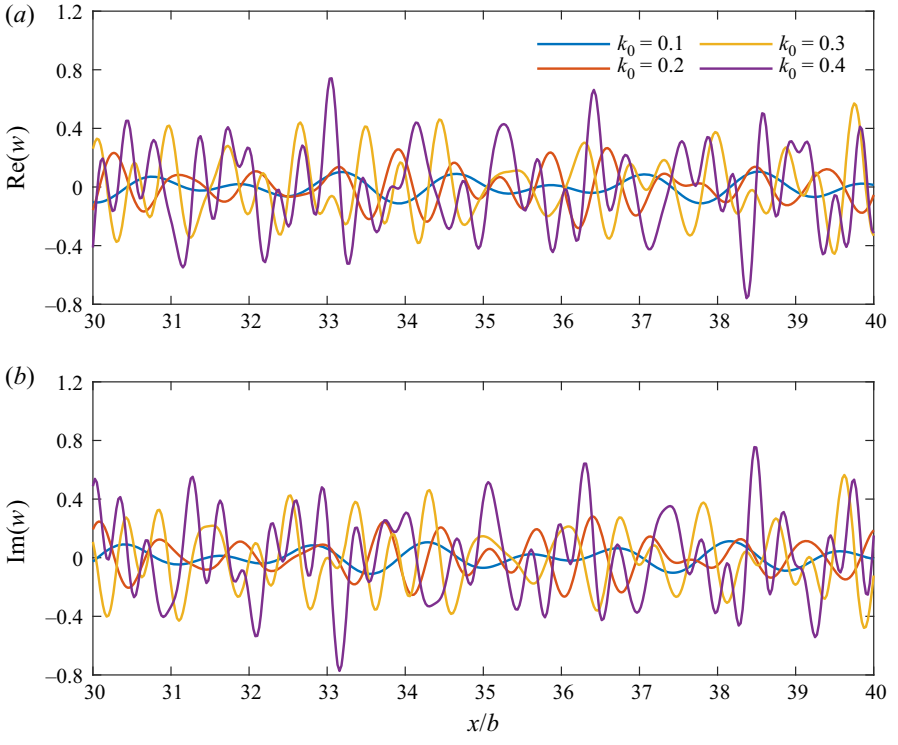

Figure 7. The wave elevation w induced by a source at $(\xi, \eta, \zeta) = (0, 0, -1)$: (*a*) real part (Re) of w_∞; (*b*) imaginary part (Im) of w_∞ ($y/b = 0$, $b = 50$, $h = 1$ m is taken as the characteristic length scale).

	$k_0 = 0.1$ with $N = 3$ ($\kappa_0 = 0.0624$)		$k_0 = 0.2$ with $N = 6$ ($\kappa_0 = 0.785$)		$k_0 = 0.3$ with $N = 10$ ($\kappa_0 = 0.0877$)		$k_0 = 0.4$ with $N = 13$ ($\kappa_0 = 0.0943$)	
j	α_j	w_j	α_j	w_j	α_j	w_j	α_j	w_j
1	0.0666	0.0501	0.1036	0.0000	0.0879	0.0000	0.1049	0.2591
2	0.0850	0.0000	0.1389	0.1182	0.1405	0.1936	0.1765	0.0000
3	0.0964	0.0630	0.1632	0.0000	0.1845	0.0000	0.2264	0.1762
4	—	—	0.1802	0.0936	0.2167	0.1315	0.2643	0.0000
5	—	—	0.1914	0.0000	0.2414	0.0000	0.2947	0.1372
6	—	—	0.1979	0.0859	0.2606	0.1105	0.3195	0.0000
7	—	—	—	—	0.2754	0.0000	0.3400	0.1196
8	—	—	—	—	0.2864	0.1010	0.3569	0.0000
9	—	—	—	—	0.2940	0.0000	0.3705	0.1101
10	—	—	—	—	0.2985	0.0971	0.3814	0.0000
11	—	—	—	—	—	—	0.3896	0.1049
12	—	—	—	—	—	—	0.3954	0.0000
13	—	—	—	—	—	—	0.3989	0.1026

Table 1. Trapped wave modes α_j at different wave number k_0 for an ice channel with half width $b = 50$. The amplitude of each wave component w_j along the longitudinal cut due to α_j is also provided ($(\xi, \eta, \zeta) = (0, 0, -1)$, $y/b = 0$, $h = 1$ m is taken as the characteristic length scale).

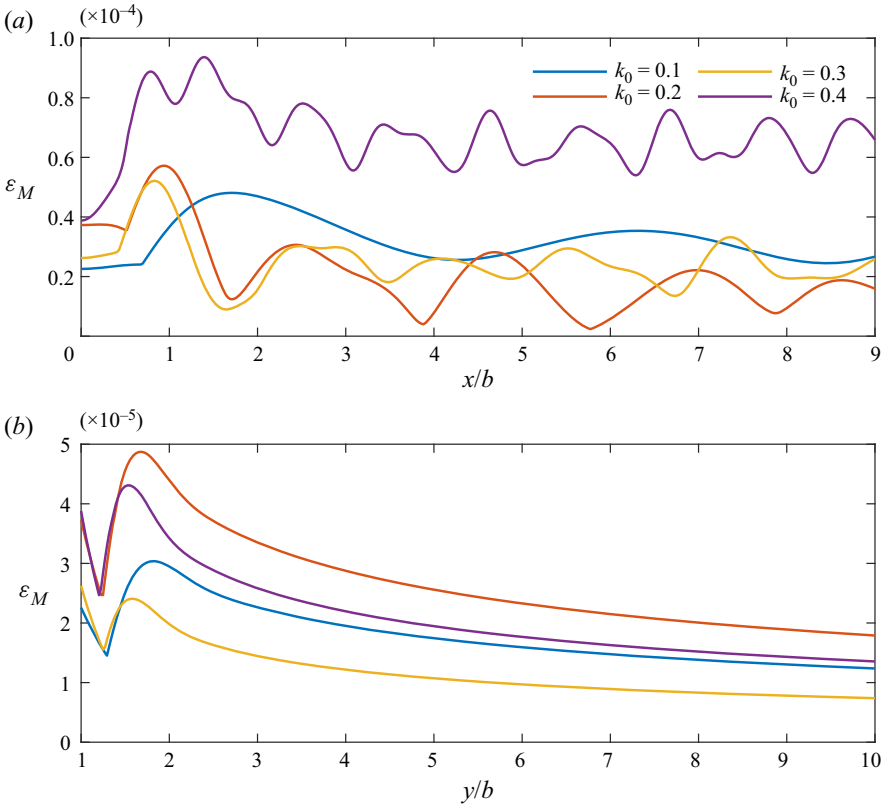

Figure 8. The maximum principal strain ε_M induced by a source at $(\xi, \eta, \zeta) = (0, 0, -1)$: (*a*) along the longitudinal cut with $y/b = 1 + 0$; (*b*) along the transverse cut with $x/b = 0$ ($b = 50$, $h = 1$ m is taken as the characteristic length scale).

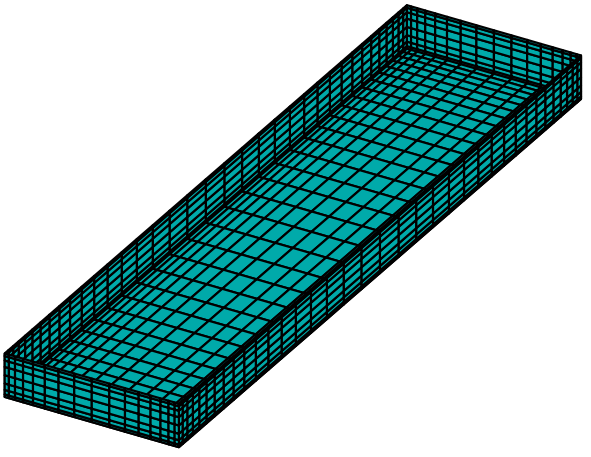

Figure 9. General view of the geometry and distribution of panels on the floating barge.

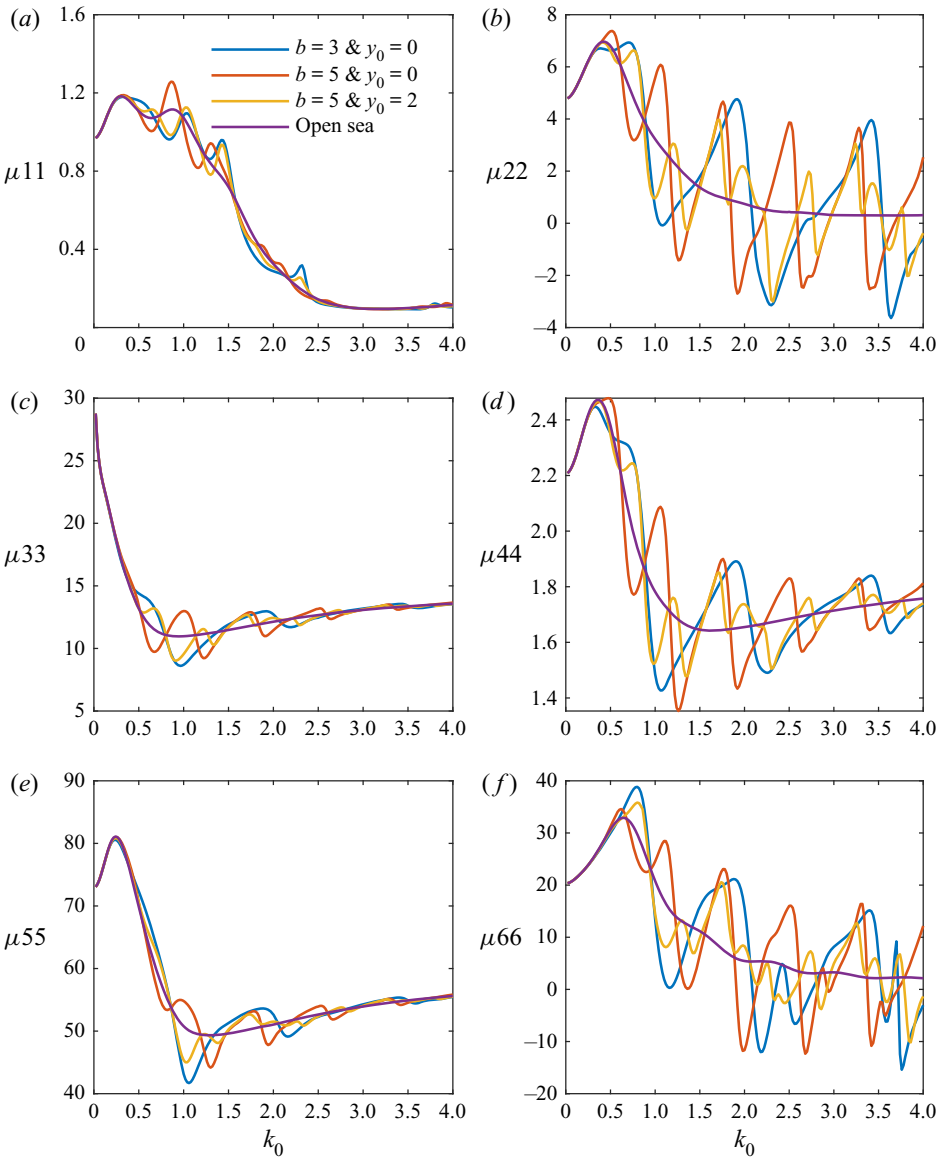

Figure 10. Added mass μ_{jj} of a barge floating on different transverse positions of the ice channel with different widths against wave number k_0 ($L_L/L_B = 4$, $D/L_B = 0.25$, $(x_0, z_0) = (0, -D/2)$, $\beta = \pi/4$, $L_B/2 = 10$ m is taken as the characteristic length scale).

As k_0 increases, the hydrodynamic forces for ice channel with different widths begin to depart from each other, and all of them show an oscillatory behaviour with k_0 and the oscillation is around the results for open sea. The problem for a barge in a channel with two solid side walls has been studied previously, and the numerical result of Newman (2017) revealed that at some discrete wave numbers the wave due to the barge oscillation would not propagate to infinity along the channel or the wave would be confined near the body. At these wave numbers, the added mass would be infinite and the damping coefficient would be zero. Here, only the free surface in the channel is confined by two semi-infinite

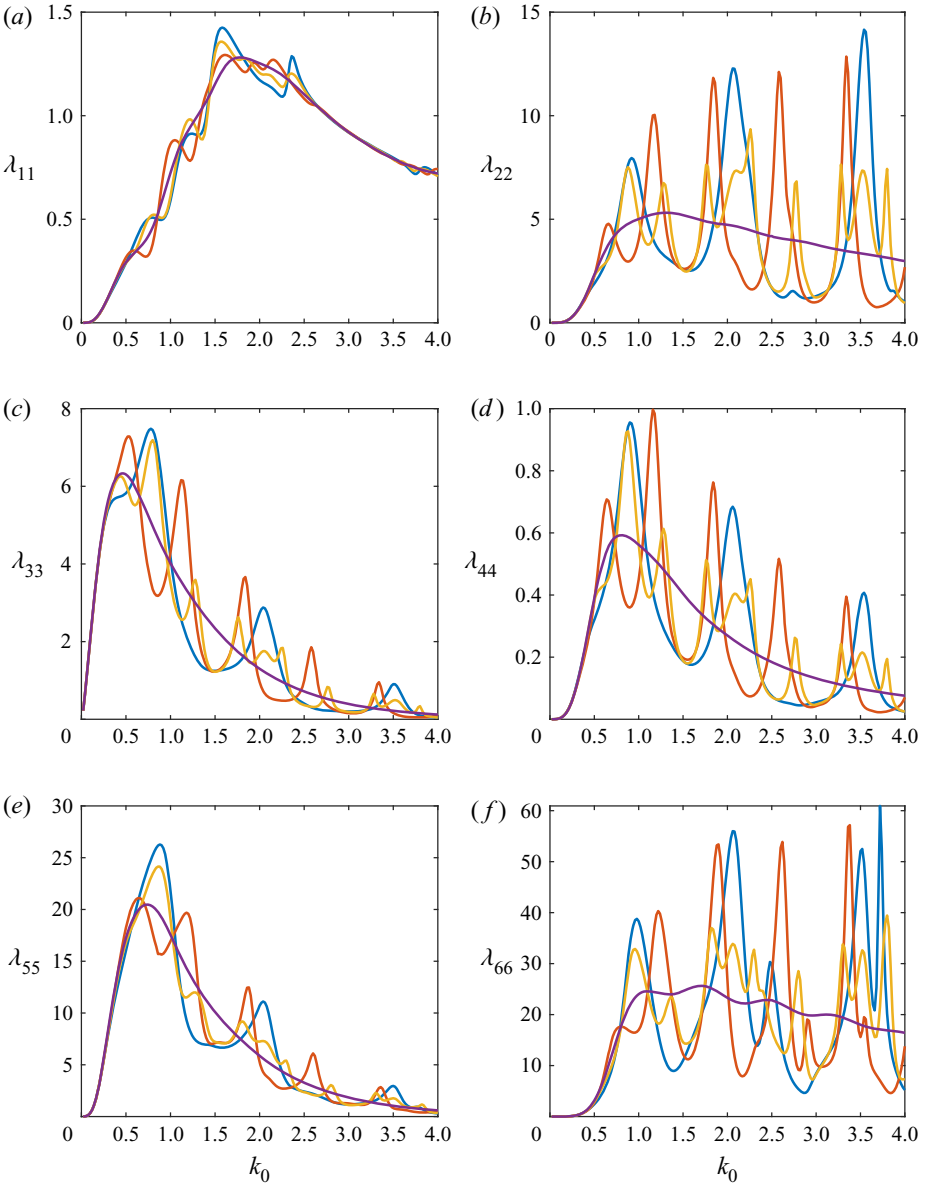

Figure 11. Damping coefficient λ_{jj} of a barge floating on different transverse positions of the ice channel with different widths against wave number k_0. See the caption of figure 10 for further information.

ice sheets, whereas the fluid domain below the surface still tends to infinity. This means that the radiated wave will propagate not only along the channel on the free surface, but also into the domain below the ice sheet. Therefore, no zero damping case is observed. On the other hand, as in the 2-D problem (Li *et al.* 2017), there will be wave motions in the channel, which may resemble a 'transverse sloshing wave', leading to the oscillatory behaviour of the results with the wave number.

As the channel width increases or the barge floats off-centrally, it can be seen from the figures that the hydrodynamic forces become more oscillatory. This may be partly

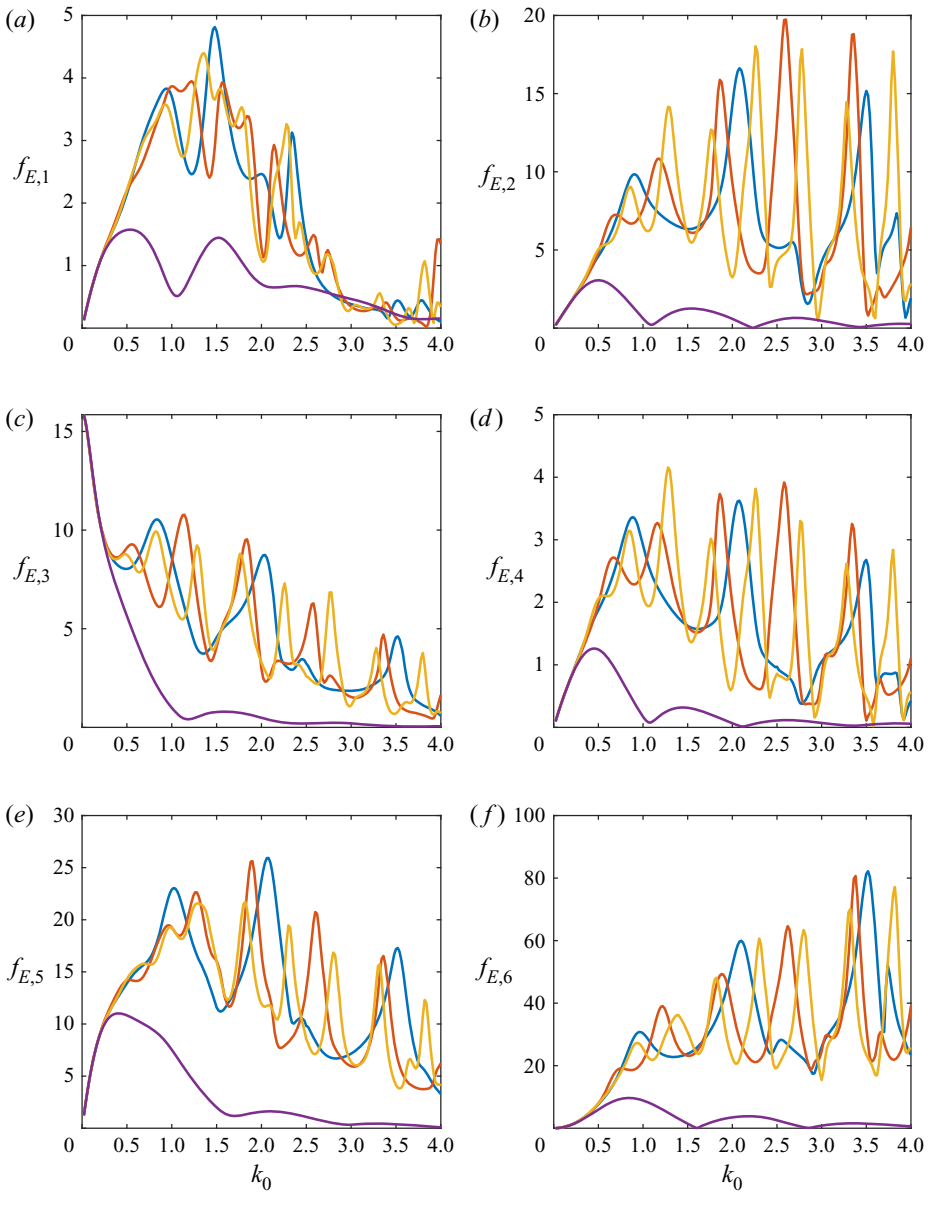

Figure 12. Wave exciting force $f_{E,j}$ on a barge floating on different transverse positions of the ice channel with different widths against wave number k_0. See the caption of figure 10 for further information.

explained by the 2-D approximate solution for a body in a wide channel (Li *et al.* 2017). The obtained explicit formulae reveal that the oscillatory behaviours of the hydrodynamic forces will depend on two parameters, namely b and y_0, or the oscillation has two periods $2k_0b$ and $2k_0|y_0|$, respectively. This indicates that at a larger b or a larger y_0, the hydrodynamic forces will oscillate more quickly with k_0, as observed in the figures.

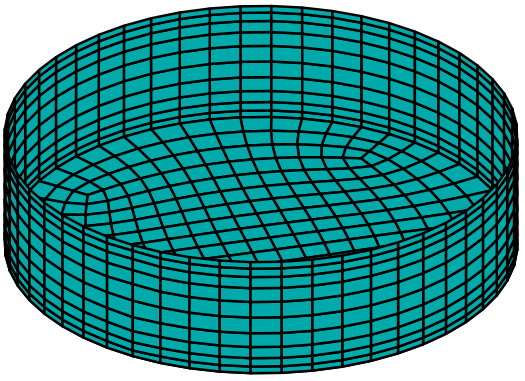

Figure 13. General view of the geometry and distribution of panels on the truncated vertical circular cylinder.

4.3. *Wave interactions with two bodies floating on the ice channel*

As discussed in § 3 and illustrated in § 4.1, a major feature of this ice channel problem is those α_j waves, which do not decay along the channel. This means when there are two bodies in the channel at the same time, the wave generated by one body will significantly affect the other, even when the distance between them is relatively large. Here, we shall undertake a case study of two bodies floating in the channel. Both bodies have the same geometry shape, i.e. a truncated vertical circular cylinder with radius a and draught D. The radius $a = 10$ m is chosen as the characteristic length scale with $D/a = 0.5$ and $b = 5$. The rotational center is taken at the geometry centre. The incident flexural gravity wave is assumed to be from $\beta = \pi/4$. The first cylinder is taken to be at $x_0^1 = 0$, whereas three positions of the second cylinder are considered, namely $x_0^2 = 2.5$, 10 and 40, respectively. Here, the superscript 1 and 2 indicate the rotational centres of the first and second cylinders, respectively. To conduct numerical computations, each cylinder surface S_B is discretized into $N_B = 845$ flat panels, as shown in figure 13, whereas the corresponding extended interior surface S_E is discretized into $N_E = 153$ flat panels. The other parameters or M_D and M_G for the truncation of infinite summations are taken to be the same as those in § 4.2. These are found to be sufficient to provide the converged hydrodynamic forces.

The computed diagonal terms of the added mass and damping coefficient in the O–xz plane for the first cylinder with $x_0^1 = 0$ are shown in figures 14 and 15, respectively, against wave number k_0. The corresponding wave exciting force is presented in figure 16. For full open water or $h = 0$, it can be observed from the figures that when there is another body at x_0^2, the hydrodynamic forces on the first body at $x_0^1 = 0$ show that results oscillate around those of a single body. The results may become more oscillatory as $x_0^2 - x_0^1$ increases. However, the amplitude of oscillation decays, which suggests the interaction between the two bodies becomes weak. This can be partially explained through the approximate formula in Srokosz & Evans (1979) based on wide spacing approximation. They showed that the results would oscillate with a period of $2k_0(x_0^2 - x_0^1)$. However, the wave generated by a body in open water will decay at the rate proportional to the square root of the distance from the body. Thus, its effect in a region far away from the body will diminish. This can be seen in figures 14–16. For the case of $x_0^2 = 40$, the results for the first cylinder are almost the same as those for a single cylinder.

In the case of the ice channel, the wave generated by the body does not always decay, because there may exist those wave components of α_j which oscillate with x periodically as shown in § 4.1. This means that as $x_0^2 - x_0^1 \to +\infty$ although the wave component with

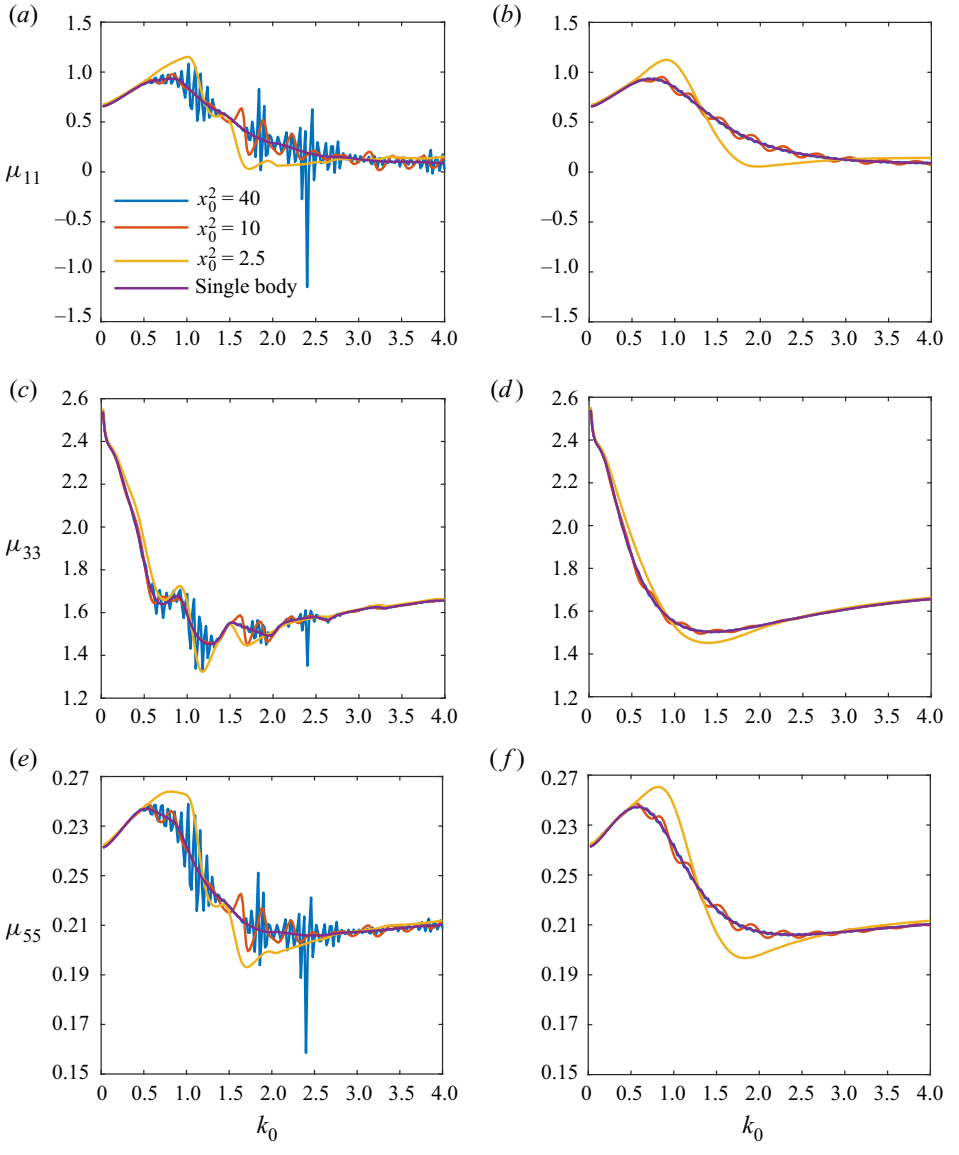

Figure 14. Added mass μ_{jj} of the first cylinder at $x_0^1 = 0$ against wave number k_0 with the second cylinder at different longitudinal position x_0^2: (*a*,*c*,*e*) ice channel; (*b*,*d*,*f*) open water ($D/a = 0.5$, $(y_0^1, z_0^1) = (0, -D/2)$, $(y_0^2, z_0^2) = (0, -D/2)$, $b = 5$, $\beta = \pi/4$, $a = 10$ m is taken as the characteristic length scale).

wave number k_0 will tend to be zero, the interactions due to the wave components of α_j will still be there. Then it can be expected that no matter how large $x_0^2 - x_0^1$ is, the interaction effect for two bodies floating on the ice channel will always be there unless $N = 0$. The interaction effect is given in figures 14–16, which show that even at $x_0^2 = 40$, the results for the first body still oscillate around those for a single body.

As can be seen in table 1, the values of α_j as well as N change with k_0. On the other hand, the interactions between the two cylinders are expected to depend very much on $k_0(x_0^2 - x_0^1)$ and $\alpha_j(x_0^2 - x_0^1), j = 1, \ldots, N$. As α_j do not form a linear relationship with k_0,

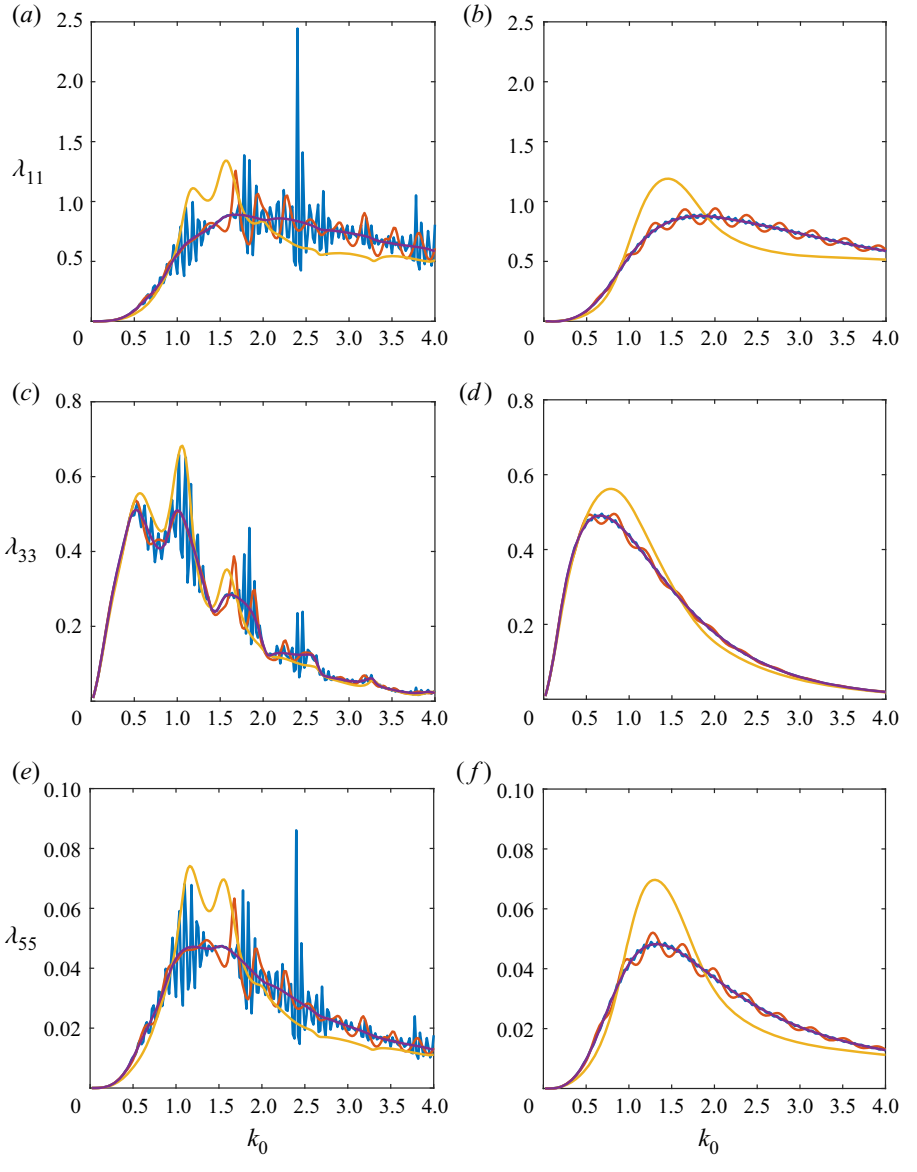

Figure 15. Damping coefficient λ_{jj} of the first cylinder at x_0^1 against wave number k_0 with the second cylinder at different longitudinal position x_0^2. See the caption of figure 14 for further information.

the oscillatory behaviours of the results due to the interaction do not change periodically with k_0. In fact, the oscillation seems to highly erratic. In some cases, several peaks and troughs are very close to each other, especially at larger $x_0^2 - x_0^1$. At larger k_0, the effect of the second cylinder on the added mass seems to have decreased significantly. The effect on damping and exciting force is, however, still rather strong. In fact, when the damping of the single cylinder is not small, it means that its generated wave is not negligible. Thus, the wave generated by one cylinder will still affect the other, or their mutual interactions will remain to be significant, as can be seen from figures 15(*a*) and 15(*e*).

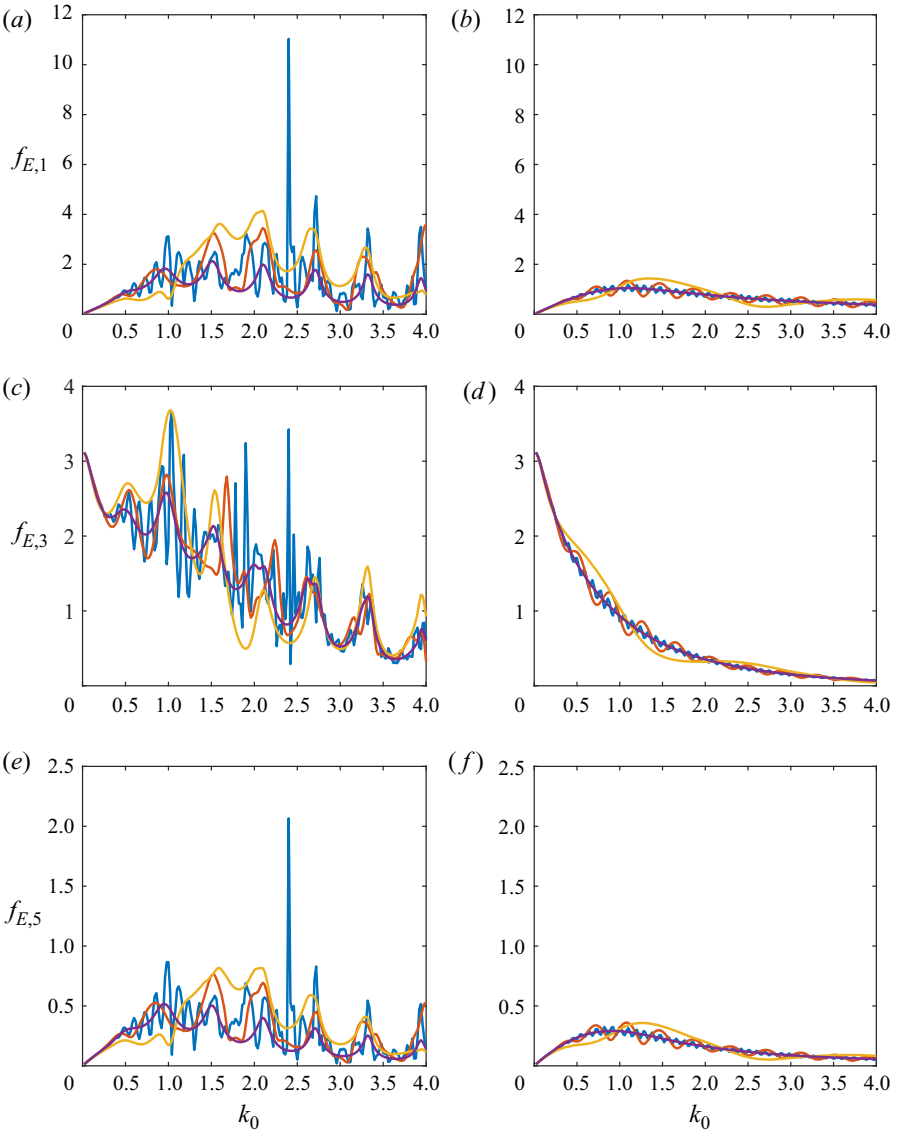

Figure 16. Wave exciting force $f_{E,j}$ on the first cylinder at x_0^1 against wave number k_0 with the second cylinder at different longitudinal position x_0^2. See the caption of figure 14 for further information.

5. Conclusions

The hydrodynamic problem of a body floating on the water surface in a channel confined by two semi-infinite ice sheets has been solved, based on the linearized velocity potential theory and thin elastic plate model. The Green function was first derived, which satisfies all the boundary conditions apart from that on the body surface. Through its integral form, singularities have been identified numerically, which correspond to the non-decaying waves propagating along the channel. With the help of this Green function, it has been found that similar to the problem without ice sheet, the differential equation for the velocity potential can be transformed into an integral equation over the body surface only, which has been solved numerically through the boundary element method.

From the solution of the Green function, it has been observed that when wave number k_0 of the free surface is larger than the wave number κ_0 of the ice sheet, there will be a number of non-decaying waves with wave numbers α_j, $j = 1, \ldots, N$, respectively, and $\kappa_0 < \alpha_1 < \ldots < \alpha_N < k_0$, which is consistent with the trapped modes found by Porter (2018) previously. These waves decay exponentially away from the channel in its transverse direction. When k_0 increases, the number N of these waves will increase and several of the largest wave numbers are quite close to k_0.

For a floating body in the channel, the usual interaction between the free surface wave and the body will be complicated by the ice sheets. Their presence leads the wave in the channel to continuously propagate outwards and inwards, causing the effects similar to that due to sloshing. This is reflected by the results of the hydrodynamic forces, which show that they will oscillate around those for open sea, and they will become more oscillatory as the channel width increases or the body is away from the channel centre. The interaction is made more complex by those non-decaying waves of α_j in the channel.

When there are multiple bodies in the channel, their mutual interactions will not decrease even when the distance between them is very large. This is mainly due to the effect of non-decaying waves in the channel. Through detailed simulations for two bodies in the channel, it is found that the hydrodynamic forces on the first body oscillate around those of a single body, and the results will become more oscillatory as their distance increases. The effect on the added mass on the first body by the second body may decrease as their distance increases. However, the effect on the wave damping remains significant, a result of the non-decaying wave in the channel.

Acknowledgements. This work is supported by Lloyd's Register Foundation, to which the authors are most grateful. Lloyd's Register Foundation helps to protect life and property by supporting engineering-related education, public engagement, and the application of research. This work is also supported by the National Natural Science Foundation of China (Grant No. 51709131, 52071162, 52025112 and 51879123).

Declaration of interests. The authors report no conflict of interest.

Author ORCIDs.
Zhi Fu Li https://orcid.org/0000-0001-7507-4176;
Guo Xiong Wu https://orcid.org/0000-0002-3652-1970;
Kang Ren https://orcid.org/0000-0002-9640-0521.

Appendix A. Special case for ice sheet with zero thickness or full free surface

When the ice thickness becomes zero or $h = 0$, $L = 0$ and (3.41) and (3.42) become

$$U_m = P_m \quad \text{and} \quad V_{m,\tilde{m}} = \delta_{m,\tilde{m}} P_m. \tag{A1a,b}$$

Then (3.48) and (3.49) give

$$c_m^+ = \frac{1}{\mathrm{i}\beta_m P_m} \exp(-\mathrm{i}\beta_m(b-\eta)) Z_m(\zeta) \quad \text{and} \quad c_m^- = \frac{1}{\mathrm{i}\beta_m P_m} \exp(-\mathrm{i}\beta_m(b+\eta)) Z_m(\zeta), \tag{A2a,b}$$

and (3.46) and (3.47) provide

$$a_m = 0 \quad \text{and} \quad b_m = 0. \tag{A3a,b}$$

This means that

$$\tilde{G} = \tilde{F} = \sum_{m=0}^{\infty} \frac{1}{\mathrm{i}\beta_m P_m} \exp(-\mathrm{i}\alpha\xi) \exp(-\mathrm{i}\beta_m |y-\eta|) Z_m(\zeta) Z_m(z), \tag{A4}$$

is valid below both the free surface and the ice sheet. Substituting $\tilde{G}$ into (3.50), we obtain

$$G = \sum_{m=0}^{\infty} \frac{1}{\mathrm{i}P_m} Z_m(\zeta) Z_m(z) \mathrm{I}_m, \tag{A5}$$

where

$$\mathrm{I}_m = \int_{-\infty}^{+\infty} \frac{1}{\beta_m} \exp(+\mathrm{i}\alpha(x-\xi)) \exp(-\mathrm{i}\beta_m |y-\eta|)\, \mathrm{d}\alpha. \tag{A6}$$

We may replace the integral variable with $\alpha = \mathrm{i}k_m \sinh t$, which gives $\beta_m = k_m \cosh t$ based on the fact that $\beta_m^2 = k_m^2 - \alpha^2$. Then for $m \geqslant 1$, i.e. when k_m is a purely negative imaginary number, equation (A6) can be rewritten as

$$\mathrm{I}_m = \mathrm{i} \int_{-\infty}^{+\infty} \exp(+\mathrm{i}\alpha(x-\xi)\mathrm{i}k_m \sinh t) \exp(-\mathrm{i}|y-\eta|k_m \cosh t)\, \mathrm{d}t. \tag{A7}$$

Letting $\mathrm{i}(x-\xi) = R\sinh t'$ and $|y-\eta| = R\cosh t'$, where $R^2 = (x-\xi)^2 + (y-\eta)^2$ and $t' = \mathrm{i}\theta \in (-\mathrm{i}\pi/2, +\mathrm{i}\pi/2)$ is a pure imaginary number, this equation can be further written as

$$\mathrm{I}_m = \mathrm{i} \int_{-\infty}^{+\infty} \exp(-\mathrm{i}k_m R \cosh(t-t'))\, \mathrm{d}t. \tag{A8}$$

Letting $k_m = -\mathrm{i}\bar{k}_m$ with $\bar{k}_m$ being real and positive, and $\tau = -\mathrm{i}(t-t')$, equation (A8) becomes

$$\mathrm{I}_m = -\int_{-\theta+\mathrm{i}\infty}^{-\theta-\mathrm{i}\infty} \exp(-\bar{k}_m R\cos\tau)\, \mathrm{d}\tau. \tag{A9}$$

From Erdélyi (1953), we have

$$\mathrm{I}_m = 2\mathrm{i}\mathrm{K}_0(\bar{k}_m R), \tag{A10}$$

where K_0 is the modified Bessel function. From (9.6.4) of Abramowitz & Stegun (1965), we further have

$$\mathrm{I}_m = \pi H_0^{(2)}(k_m R). \tag{A11}$$

For $m = 0$, i.e. k_0 is a purely positive real number, t must be a complex number if we write $\alpha = \mathrm{i}k_m \sinh t$. When the integral route for α is from $-\infty$ to $+\infty$ along the real axis, the route C for t is shown in figure 17. Substituting this into (A6), we have

$$\mathrm{I}_0 = \mathrm{i} \int_C \exp(-\mathrm{i}k_0 R \cosh(t-t'))\, \mathrm{d}t. \tag{A12}$$

Letting $\tau = -\mathrm{i}(t-t') + \pi$, we have

$$\mathrm{I}_0 = -\int_{\tilde{C}} \exp(+\mathrm{i}k_0 R\cos\tau)\, \mathrm{d}\tau, \tag{A13}$$

where the integral route $\tilde{C}$ is shown in figure 17 with $a \in (\pi, 2\pi)$ and $b \in (0, \pi)$. From Erdélyi (1953), we have

$$\mathrm{I}_0 = \pi H_0^{(2)}(k_0 R). \tag{A14}$$

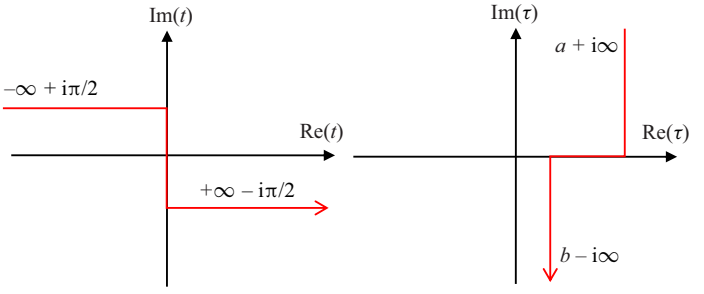

Figure 17. Integral route C for t in (A12) and $\tilde{G}$ for τ in (A13).

Based on (A11) and (A14), we then have that the Green function G in (A4) is identical to that for free surface, or (Li *et al.* 2020*a*)

$$G = \sum_{m=0}^{\infty} \frac{1}{\mathrm{i}P_m} Z_m(\zeta) Z_m(z) \pi H_0^{(2)}(k_m R). \tag{A15}$$

It should be noted that (A15) can be also written in an integral form as (Wehausen & Laitone 1960)

$$G = \frac{1}{r_1} + \frac{1}{r_2} + 2\int_0^{+\infty} \mathrm{e}^{-kH} \frac{gk+\omega^2}{\mathrm{K}_1(\omega,k)} \frac{\cosh[k(\zeta+H)]}{\cosh(kH)} \cosh[k(z+H)]\mathrm{J}_0(kR)\,\mathrm{d}k, \tag{A16}$$

where the integral route from 0 to $+\infty$ should pass over the pole at $k = k_0$, r_1 is the distance between p and q, r_2 is the distance between p and the mirror image of q about the flat seabed, $\mathrm{J}_0(kR)$ is the zeroth-order Bessel function of first kind (Abramowitz & Stegun 1965), with R as the horizontal distance between p and q.

Appendix B. Boundary integral equation for the disturbed velocity potential

To obtain the boundary integral equation for the disturbed velocity potential, we first show the symmetry property of the Green function regarding the source and field points. Assuming $G^a(p, q^a)$ and $G^b(p, q^b)$ are two solutions to the governing equation (3.1) for sources located at q^a and q^b, respectively. Applying Green's second identity to them, we have

$$\begin{aligned} &-4\pi[G^a(q^b, q^a) - G^b(q^a, q^b)] \\ &\quad = \int_S \left[G^a(p, q^a) \frac{\partial G^b(p, q^b)}{\partial n_p} - \frac{\partial G^a(p, q^a)}{\partial n_p} G^b(p, q^b) \right] \mathrm{d}s_p, \end{aligned} \tag{B1}$$

where the fluid boundary S includes the ice sheet S_I^+ (S_I^-) for $y \geqslant b + 0$ ($y \leqslant -b - 0$), free surface S_F in the channel bounded by $y = b - 0$ and $y = -b + 0$, sea bed S_H and a vertical rectangular surface S_∞ at infinity. For the full free surface problem, the right-hand side of (B1) can be easily found to be zero when the boundary conditions are used. However, for the present problem, this is far less straightforward because of complex ice sheet condition and multiple wave components at $x = \pm\infty$. Therefore, rigorous proof is needed.

As discussed following equation (3.55), the wave components of α_j decay exponentially with respect to y. Thus, the leading term will be that due to the ring wave (Li *et al.* 2020*a*), which is in the form of $\exp(-\mathrm{i}\kappa_0 R)/\sqrt{R}$ with $R = \sqrt{x^2 + y^2}$. Using this, it can be seen that

the contribution from $y=\pm\infty$ in (B1) is zero. The boundary conditions (2.4) and (2.13) provide that the integral over S_F and S_H equal zero. Invoking the boundary condition (2.8) on $S_I^{\pm}$, we have

$$G=\frac{L}{\rho_w\omega^2}\nabla^2\frac{\partial G}{\partial z}+\frac{\rho_w g-m_i\omega^2}{\rho_w\omega^2}\frac{\partial G}{\partial z}, \tag{B2}$$

where G can be either G^a or G^b. Substituting (B2) into (B1) and then applying the Gauss's theorem, we obtain (Li *et al.* 2018*c*)

$$\int_{S_I^+}\left(G^a\frac{\partial G^b}{\partial n_p}-\frac{\partial G^a}{\partial n_p}G^b\right)\mathrm{d}s_p=I^{b+}+I^{n+}-I^{n-}, \tag{B3}$$

for $y\geqslant b+0$, where

$$I^{b+}=-\frac{L}{\rho_w\omega^2}\int_{-\infty}^{+\infty}\left(\frac{\partial^3 G^a}{\partial z^3}\frac{\partial^2 G^b}{\partial z\partial y}+\frac{\partial G^a}{\partial z}\frac{\partial^4 G^b}{\partial z^3\partial y}-\frac{\partial^3 G^b}{\partial z^3}\frac{\partial^2 G^a}{\partial z\partial y}-\frac{\partial G^b}{\partial z}\frac{\partial^4 G^a}{\partial z^3\partial y}\right)_{z=0,y=b+0}\mathrm{d}x, \tag{B4}$$

$$I^{n\pm}=\frac{L}{\rho_w\omega^2}\int_{b+0}^{+\infty}\left(\frac{\partial^3 G^a}{\partial z^3}\frac{\partial^2 G^b}{\partial z\partial x}+\frac{\partial G^a}{\partial z}\frac{\partial^4 G^b}{\partial z^3\partial x}-\frac{\partial^3 G^b}{\partial z^3}\frac{\partial^2 G^a}{\partial z\partial x}-\frac{\partial G^b}{\partial z}\frac{\partial^4 G^a}{\partial z^3\partial x}\right)_{z=0,x=\pm\infty}\mathrm{d}y. \tag{B5}$$

Here, the line integral at $y=+\infty$ is zero and has been removed. The free ice edge conditions (2.9) provide

$$\frac{\partial^3 G}{\partial z^3}=-\nabla^2\frac{\partial G}{\partial z}=-(1-\nu)\frac{\partial^3 G}{\partial x^2\partial z}\quad\text{and}\quad\frac{\partial^4}{\partial z^3\partial y}=-\nabla^2\frac{\partial^2 G}{\partial y\partial z}=(1-\nu)\frac{\partial^4 G}{\partial y\partial x^2\partial z}, \tag{B6a,b}$$

for $|y|=b+0$ and $z=0$. Substituting (B6*a*,*b*) into (B4), we obtain

$$I^{b+}=I^{b+}_{x+}-I^{b+}_{x-}, \tag{B7}$$

where

$$I^{b+}_{x\pm}=\frac{L(1-\nu)}{\rho_w\omega^2}\frac{\partial}{\partial y}\left[\left(\frac{\partial^2 G^a}{\partial x\partial z}\frac{\partial G^b}{\partial z}-\frac{\partial G^a}{\partial z}\frac{\partial^2 G^b}{\partial x\partial z}\right)_{x=\pm\infty}\right]. \tag{B8}$$

Invoking (3.55), at $x=+\infty$ we may write G as

$$G^a=\sum_{j=0}^{N}G^a_j(y,z)\,\mathrm{e}^{-\mathrm{i}\alpha_j x}\quad\text{and}\quad G^b=\sum_{k=0}^{N}G^b_k(y,z)\,\mathrm{e}^{-\mathrm{i}\alpha_k x}. \tag{B9a,b}$$

Here, α_j $(j=1,\ldots,N)$ correspond to the first-order singularities of $\tilde{G}$ in (3.50), and G^a_j and G^b_k does not decay at $x=\pm\infty$. While $\alpha_0=k_0$ with $|y|\leqslant b-0$ ($\alpha_0=\kappa_0$ with $|y|\geqslant b+0$) corresponds to the square root singularity of $\tilde{G}$, and G^a_0 and G^b_0 decay in the form of $1/\sqrt{|x|}$ as $x=\pm\infty$, which can be reflected by the Hankel function equation (3.53). Strictly speaking, G^a_0 and G^b_0 are also functions of x. However, as $\mathrm{d}G^a_0/\mathrm{d}x$ and $\mathrm{d}G^b_0/\mathrm{d}x$ are

of higher order of x, they have been written as functions of y and z only. The remaining terms in G decay in a higher order form, and their contribution to (B1) will be zero. The substitution of (B9*a*,*b*) into (B8) gives

$$I_{x+}^{b+} = \mathrm{i}\frac{L(1-\nu)}{\rho_w\omega^2}\sum_{j=1}^{N}\sum_{\substack{k=1\\k\neq j}}^{N}(\alpha_k-\alpha_j)\exp(-\mathrm{i}(\alpha_j+\alpha_k)x)\left(\frac{\partial^2 G_j^a}{\partial y\partial z}\frac{\partial G_k^b}{\partial z}+\frac{\partial G_j^a}{\partial z}\frac{\partial^2 G_k^b}{\partial y\partial z}\right)$$

$$= \mathrm{i}\frac{L(1-\nu)}{\rho_w\omega^2}\sum_{j=1}^{N}\sum_{\substack{k=1\\k\neq j}}^{N}\frac{\exp(-\mathrm{i}(\alpha_j+\alpha_k)x)}{\alpha_j+\alpha_k}$$

$$\times\left(\alpha_k^2\frac{\partial^2 G_j^a}{\partial y\partial z}\frac{\partial G_k^b}{\partial z}-\alpha_j^2\frac{\partial^2 G_j^a}{\partial y\partial z}\frac{\partial G_k^b}{\partial z}+\alpha_k^2\frac{\partial G_j^a}{\partial z}\frac{\partial^2 G_k^b}{\partial y\partial z}-\alpha_j^2\frac{\partial G_j^a}{\partial z}\frac{\partial^2 G_k^b}{\partial y\partial z}\right). \tag{B10}$$

It should be noted that each jth or kth term in (B9*a*,*b*) should satisfy the ice edge conditions (B6*a*,*b*) at $x=+\infty$, with the double derivatives with respect to x being replaced by $-\alpha_j^2$ or $-\alpha_k^2$. Thus, we can rewrite (B10) as

$$I_{x+}^{b+} = \mathrm{i}\frac{L}{\rho_w\omega^2}\sum_{j=1}^{N}\sum_{\substack{k=1\\k\neq j}}^{N}\frac{\exp(-\mathrm{i}(\alpha_j+\alpha_k)x)}{\alpha_j+\alpha_k}$$

$$\times\left(\frac{\partial^2 G_j^a}{\partial y\partial z}\frac{\partial^3 G_k^b}{\partial z^3}+\frac{\partial^4 G_j^a}{\partial y\partial z^3}\frac{\partial G_k^b}{\partial z}-\frac{\partial G_j^a}{\partial z}\frac{\partial^4 G_k^b}{\partial y\partial z^3}-\frac{\partial^3 G_j^a}{\partial z^3}\frac{\partial^2 G_k^b}{\partial y\partial z}\right). \tag{B11}$$

Substituting (B9*a*,*b*) into (B5), we have

$$I^{n+} = \mathrm{i}\frac{L}{\rho_w\omega^2}\sum_{j=1}^{N}\sum_{\substack{k=1\\k\neq j}}^{N}\frac{\exp(-\mathrm{i}(\alpha_j+\alpha_k)x)}{\alpha_j+\alpha_k}$$

$$\times\int_{b+0}^{+\infty}\left(\alpha_j^2\frac{\partial^3 G_j^a}{\partial z^3}\frac{\partial G_k^b}{\partial z}-\alpha_k^2\frac{\partial^3 G_j^a}{\partial z^3}\frac{\partial G_k^b}{\partial z}+\alpha_j^2\frac{\partial G_j^a}{\partial z}\frac{\partial^3 G_k^b}{\partial z^3}-\alpha_k^2\frac{\partial G_j^a}{\partial z}\frac{\partial^3 G_k^b}{\partial z^3}\right)\mathrm{d}y. \tag{B12}$$

On S_∞ in (B1), we have

$$\int_{S_\infty}\left(G^a\frac{\partial G^b}{\partial n_p}-\frac{\partial G^a}{\partial n_p}\right)\mathrm{d}s_p = J_{x+}-J_{x-}, \tag{B13}$$

where

$$J_{x\pm} = \int_{-\infty}^{+\infty}\int_{-H}^{0}\left(G^a\frac{\partial G^b}{\partial x}-\frac{\partial G^a}{\partial x}G^b\right)_{x=\pm\infty}\mathrm{d}z\,\mathrm{d}y, \tag{B14}$$

Here, the integrals at $y=\pm\infty$ are zero and have been removed. From (B9*a*,*b*), at $x=+\infty$ we have

$$G^a\frac{\partial G^b}{\partial x}-\frac{\partial G^a}{\partial x}G^b = \mathrm{i}\sum_{j=1}^{N}\sum_{\substack{k=1\\k\neq j}}^{N}(\alpha_j-\alpha_k)G_j^aG_k^b\exp(-\mathrm{i}(\alpha_j+\alpha_k)x). \tag{B15}$$

As G satisfies the Laplace equation, from (B9*a*,*b*), we have

$$\nabla_{yz}^2 G_j^a = \alpha_j^2 G_j^a \quad \text{and} \quad \nabla_{yz}^2 G_k^b = \alpha_k^2 G_k^b, \tag{B16a,b}$$

where $\nabla_{yz}^2 = \partial^2/\partial y^2 + \partial^2/\partial z^2$ is the Laplacian in the O–yz plane. From (B16*a*,*b*), we obtain

$$G_j^a G_k^b = \frac{\nabla_{yz}(G_j^a \nabla_{yz} G_k^b - G_k^b \nabla_{yz} G_j^a)}{\alpha_k^2 - \alpha_j^2}. \tag{B17}$$

Substitution of (B17) into (B15) provides

$$G^a \frac{\partial G^b}{\partial x} - \frac{\partial G^a}{\partial x} G^b = \mathrm{i} \sum_{j=1}^{N} \sum_{\substack{k=1 \\ k \neq j}}^{N} \frac{\exp(-\mathrm{i}(\alpha_j + \alpha_k)x)}{\alpha_j + \alpha_k} \nabla_{yz}(G_k^b \nabla_{yz} G_j^a - G_j^a \nabla_{yz} G_k^b). \tag{B18}$$

Invoking (B18), we may write J_{x+} in (B14) as

$$J_{x+} = \mathrm{i} \sum_{j=1}^{N} \sum_{\substack{k=1 \\ k \neq j}}^{N} \frac{\exp(-\mathrm{i}(\alpha_j + \alpha_k)x)}{\alpha_j + \alpha_k} \int_{-\infty}^{+\infty} \int_{-H}^{0} \nabla_{yz}(G_k^b \nabla_{yz} G_j^a - G_j^a \nabla_{yz} G_k^b)\, \mathrm{d}z\, \mathrm{d}y, \tag{B19}$$

or

$$J_{x+} = J_{x+}^{b+} + J_{x+}^{b-}, \tag{B20}$$

where

$$J_{x+}^{b+} = \mathrm{i} \sum_{j=1}^{N} \sum_{\substack{k=1 \\ k \neq j}}^{N} \frac{\exp(-\mathrm{i}(\alpha_j + \alpha_k)x)}{\alpha_j + \alpha_k} \int_{b+0}^{+\infty} \left(\frac{\partial G_j^a}{\partial z} G_k^b - G_j^a \frac{\partial G_k^b}{\partial z} \right)_{z=0} \mathrm{d}y, \tag{B21}$$

$$J_{x+}^{b-} = \mathrm{i} \sum_{j=1}^{N} \sum_{\substack{k=1 \\ k \neq j}}^{N} \frac{\exp(-\mathrm{i}(\alpha_j + \alpha_k)x)}{\alpha_j + \alpha_k} \int_{-\infty}^{-b-0} \left(\frac{\partial G_j^a}{\partial z} G_k^b - G_j^a \frac{\partial G_k^b}{\partial z} \right)_{z=0} \mathrm{d}y. \tag{B22}$$

Here, the boundary conditions (2.4) and (2.13) have been used to remove integral over the corresponding boundaries. Applying the ice sheet condition (2.8) to (B9*a*,*b*), we have

$$G_j^a = \frac{L}{\rho_w \omega^2} \left(\alpha_j^2 - \frac{\partial^2}{\partial y^2} \right)^2 \frac{\partial G_j^a}{\partial z} + \frac{\rho_w g - m_i \omega^2}{\rho_w \omega^2} \frac{\partial G_j^a}{\partial z}, \tag{B23}$$

$$G_k^b = \frac{L}{\rho_w \omega^2} \left(\alpha_k^2 - \frac{\partial^2}{\partial y^2} \right)^2 \frac{\partial G_k^b}{\partial z} + \frac{\rho_w g - m_i \omega^2}{\rho_w \omega^2} \frac{\partial G_k^b}{\partial z}. \tag{B24}$$

Replacing G_j^a and G_k^b in (B21) with (B23) and (B24), respectively, we have

$$J_{x+}^{b+} = P_{x+}^{b+} + Q_{x+}^{b+}, \tag{B25}$$

where

$$P^{b+}_{x+} = \mathrm{i}\frac{L}{\rho_w\omega^2}\sum_{j=1}^{N}\sum_{\substack{k=1\\k\neq j}}^{N}\frac{\exp(-\mathrm{i}(\alpha_j+\alpha_k)x)}{\alpha_j+\alpha_k} \times\int_{b+0}^{+\infty}\left(\alpha_k^4\frac{\partial G_j^a}{\partial z}\frac{\partial G_k^b}{\partial z}-2\alpha_k^2\frac{\partial G_j^a}{\partial z}\frac{\partial^3 G_k^b}{\partial y^2\partial z}-\alpha_j^4\frac{\partial G_j^a}{\partial z}\frac{\partial G_k^b}{\partial z}+2\alpha_j^2\frac{\partial^3 G_j^a}{\partial y^2\partial z}\frac{\partial G_k^b}{\partial z}\right)\mathrm{d}y, \tag{B26}$$

$$Q^{b+}_{x+} = \mathrm{i}\frac{L}{\rho_w\omega^2}\sum_{j=1}^{N}\sum_{\substack{k=1\\k\neq j}}^{N}\frac{\exp(-\mathrm{i}(\alpha_j+\alpha_k)x)}{\alpha_j+\alpha_k}\int_{b+0}^{+\infty}\left(\frac{\partial G_j^a}{\partial z}\frac{\partial^5 G_k^b}{\partial y^4\partial z}-\frac{\partial^5 G_j^a}{\partial y^4\partial z}\frac{\partial G_k^b}{\partial z}\right)\mathrm{d}y. \tag{B27}$$

Applying integration by parts to equation (B27), we have

$$Q^{b+}_{x+} = \mathrm{i}\frac{L}{\rho_w\omega^2}\sum_{j=1}^{N}\sum_{\substack{k=1\\k\neq j}}^{N}\frac{\exp(-\mathrm{i}(\alpha_j+\alpha_k)x)}{\alpha_j+\alpha_k} \times\left(\frac{\partial^4 G_j^a}{\partial y^3\partial z}\frac{\partial G_k^b}{\partial z}-\frac{\partial G_j^a}{\partial z}\frac{\partial^4 G_k^b}{\partial y^3\partial z}+\frac{\partial^2 G_j^a}{\partial y\partial z}\frac{\partial^3 G_k^b}{\partial y^2\partial z}-\frac{\partial^3 G_j^a}{\partial y^2\partial z}\frac{\partial^2 G_k^b}{\partial y\partial z}\right)_{y=b+0}. \tag{B28}$$

Invoking (B16*a*,*b*) or

$$\frac{\partial^2 G_j^a}{\partial y^2}=\alpha_j^2 G_j^a-\frac{\partial^2 G_j^a}{\partial z^2}\quad\text{and}\quad\frac{\partial^2 G_k^b}{\partial y^2}=\alpha_k^2 G_k^b-\frac{\partial^2 G_k^b}{\partial z^2}, \tag{B29a,b}$$

we can write Q^{b+}_{x+} in (B28) as

$$\begin{aligned}Q^{b+}_{x+} = {}&\mathrm{i}\frac{L}{\rho_w\omega^2}\sum_{j=1}^{N}\sum_{\substack{k=1\\k\neq j}}^{N}\frac{\exp(-\mathrm{i}(\alpha_j+\alpha_k)x)}{\alpha_j+\alpha_k} \times\left(\alpha_j^2\frac{\partial^2 G_j^a}{\partial y\partial z}\frac{\partial G_k^b}{\partial z}-\alpha_k^2\frac{\partial G_j^a}{\partial z}\frac{\partial^2 G_k^b}{\partial y\partial z}+\alpha_k^2\frac{\partial^2 G_j^a}{\partial y\partial z}\frac{\partial G_k^b}{\partial z}-\alpha_j^2\frac{\partial G_j^a}{\partial z}\frac{\partial^2 G_k^b}{\partial y\partial z}\right)\\ &-\mathrm{i}\frac{L}{\rho_w\omega^2}\sum_{j=1}^{N}\sum_{\substack{k=1\\k\neq j}}^{N}\frac{\exp(-\mathrm{i}(\alpha_j+\alpha_k)x)}{\alpha_j+\alpha_k} \times\left(\frac{\partial^4 G_j^a}{\partial y\partial z^3}\frac{\partial G_k^b}{\partial z}-\frac{\partial G_j^a}{\partial z}\frac{\partial^4 G_k^b}{\partial y\partial z^3}+\frac{\partial^2 G_j^a}{\partial y\partial z}\frac{\partial^3 G_k^b}{\partial z^3}-\frac{\partial^3 G_j^a}{\partial z^3}\frac{\partial^2 G_k^b}{\partial y\partial z}\right).\end{aligned} \tag{B30}$$

Applying (B29*a*,*b*) to (B26) and using integration by parts, we have

$$
\begin{aligned}
P_{x+}^{b+} &= \mathrm{i}\frac{L}{\rho_w\omega^2}\sum_{j=1}^{N}\sum_{\substack{k=1\\k\neq j}}^{N}\frac{\exp(-\mathrm{i}(\alpha_j+\alpha_k)x)}{\alpha_j+\alpha_k}\\
&\quad\times\int_{b+0}^{+\infty}\left(\alpha_k^2\frac{\partial G_j^a}{\partial z}\frac{\partial^3 G_k^b}{\partial z^3}-\alpha_j^2\frac{\partial^3 G_j^a}{\partial z^3}\frac{\partial G_k^b}{\partial z}+\alpha_j^2\frac{\partial G_j^a}{\partial z}\frac{\partial^3 G_k^b}{\partial y^2\partial z}-\alpha_k^2\frac{\partial^3 G_j^a}{\partial y^2\partial z}\frac{\partial G_k^b}{\partial z}\right)\mathrm{d}y\\
&\quad+\mathrm{i}\frac{L}{\rho_w\omega^2}\sum_{j=1}^{N}\sum_{\substack{k=1\\k\neq j}}^{N}\frac{\exp(-\mathrm{i}(\alpha_j+\alpha_k)x)}{\alpha_j+\alpha_k}\\
&\quad\times\left(\alpha_j^2\frac{\partial G_j^a}{\partial z}\frac{\partial^2 G_k^b}{\partial y\partial z}-\alpha_k^2\frac{\partial^2 G_j^a}{\partial y\partial z}\frac{\partial G_k^b}{\partial z}-\alpha_j^2\frac{\partial^2 G_j^a}{\partial y\partial z}\frac{\partial G_k^b}{\partial z}+\alpha_k^2\frac{\partial G_j^a}{\partial z}\frac{\partial^2 G_k^b}{\partial y\partial z}\right)_{y=b+0}.
\end{aligned}
\tag{B31}
$$

Taking summation of (B11), (B12), (B30) and (B31), we have

$$
\begin{aligned}
&I_{x+}^{b+}+I^{n+}+J_{x+}^{b+}\\
&\quad=\mathrm{i}\frac{L}{\rho_w\omega^2}\sum_{j=1}^{N}\sum_{\substack{k=1\\k\neq j}}^{N}\frac{\exp(-\mathrm{i}(\alpha_j+\alpha_k)x)}{\alpha_j+\alpha_k}\\
&\quad\times\int_{b+0}^{+\infty}\left[\alpha_j^2\frac{\partial G_j^a}{\partial z}\left(\frac{\partial^3 G_k^b}{\partial y^2\partial z}+\frac{\partial^3 G_k^b}{\partial z^3}\right)-\alpha_k^2\frac{\partial G_k^b}{\partial z}\left(\frac{\partial^3 G_j^a}{\partial y^2\partial z}+\frac{\partial^3 G_j^a}{\partial z^3}\right)\right]\mathrm{d}y.
\end{aligned}
\tag{B32}
$$

Invoking (B29*a*,*b*), we further have

$$
I_{x+}^{b+}+I^{n+}+J_{x+}^{b+}=0. \tag{B33}
$$

Similar results can be obtained for $x=+\infty$ and $y\leqslant -b-0$, $x=-\infty$ and $y\geqslant b+0$, $x=-\infty$ and $y\leqslant -b-0$. This indicates that the summation of the integrals over S_I^+, S_I^- and S_∞ equal zero, i.e.

$$
G^a(q^b,q^a)=G^b(q^a,q^b). \tag{B34}
$$

Similar to (B1), we may apply Green's second identity to the disturbed velocity potential ϕ and the Green function G, and obtain

$$
\ell\phi(p)=\int_S\left[G(p,q)\frac{\partial\phi(q)}{\partial n_q}-\frac{\partial G(p,q)}{\partial n_q}\phi(q)\right]\mathrm{d}s_q, \tag{B35}
$$

where $S=S_I^+ + S_I^- + S_F + S_H + S_\infty + S_B$ with S_B as the body surface, and α is the solid angle at point p. As ϕ satisfies the same boundary conditions as G on S_I^+, S_I^-, S_F and S_H, and has the same asymptotic forms at S_∞, then by following similar procedure to obtain (B34), we have that only the integral over S_B is non-zero, or

$$
\ell\phi(p)=\int_{S_B}\left[G(p,q)\frac{\partial\phi(q)}{\partial n_q}-\frac{\partial G(p,q)}{\partial n_q}\phi(q)\right]\mathrm{d}s_q. \tag{B36}
$$

References

Abramowitz, M. & Stegun, I.A. 1965 *Handbook of Mathematical Functions*. Dover Press.

Appolonov, E.M., Sazonov, K.E., Dobrodeev, A.A., Klementieva, N.Y., Kudrin, M.A., Maslich, E.A., Petinov, V.O. & Shaposhnikov, V.M. 2013 Studies for development of technologies to make a wide channel in ice. In *The 22nd International Conference on Port and Ocean Engineering under Arctic Conditions*. 9–13 June, Espoo, Finland.

Bennetts, L.G. & Williams, T.D. 2010 Wave scattering by ice floes and polynyas of arbitrary shape. *J. Fluid Mech.* **662**, 5–35.

Chung, H. & Linton, C.M. 2005 Reflection and transmission of waves across a gap between two semi-infinite elastic plates on water. *Q. J. Mech. Appl. Maths* **58**, 1–15.

Eatock Taylor, R. & Hung, S.M. 1985 Mean drift forces on an articulated column oscillating in a wave tank. *Appl. Ocean Res.* **7**, 66–78.

Erdélyi, A. 1953 *Higher Transcendental Functions*. McGraw-Hill.

Lee, C.H., Newman, J.N. & Zhu, X. 1996 An extended boundary integral equation method for the removal of irregular frequency effects. *Intl J. Numer. Meth. Fluids* **23**, 637–660.

Li, Z.F., Shi, Y.Y. & Wu, G.X. 2017 Interaction of wave with a body floating on a wide polynya. *Phys. Fluids* **29**, 097104.

Li, Z.F., Shi, Y.Y. & Wu, G.X. 2018*a* Interaction of waves with a body floating on polynya between two semi-infinite ice sheets. *J. Fluids Struct.* **78**, 86–108.

Li, Z.F., Shi, Y.Y. & Wu, G.X. 2020*a* A hybrid method for linearized wave radiation and diffraction problem by a three dimensional floating structure in a polynya. *J. Comput. Phys.* **412**, 109445.

Li, Z.F., Wu, G.X. & Ji, C.Y. 2018*b* Wave radiation and diffraction by a circular cylinder submerged below an ice sheet with a crack. *J. Fluid Mech.* **845**, 682–712.

Li, Z.F., Wu, G.X. & Ren, K. 2020*b* Wave diffraction by multiple arbitrary shaped cracks in an infinitely extended ice sheet of finite water depth. *J. Fluid Mech.* **893**, A14.

Li, Z.F., Wu, G.X. & Shi, Y.Y. 2018*c* Wave diffraction by a circular crack in an ice sheet floating on water of finite depth. *Phys. Fluids* **30**, 117103.

Lighthill, J. 1978 *Waves in Fluids*. Cambridge University Press.

Linton, C.M. 1999 A new representation for the free-surface channel Green's function. *Appl. Ocean Res.* **21**, 17–25.

Linton, C.M. & Evans, D.V 1992 The radiation and scattering of surface waves by a vertical circular cylinder in a channel. *Phil. Trans. R. Soc. Lond.* A **338**, 325–357.

Newman, J.N. 1977 *Marine Hydrodynamics*. MIT Press.

Newman, J.N. 2016 Channel wall effects in radiation-diffraction analysis. In *The 31st International Workshop on Water Waves and Floating Bodies*. 3–6 April, Plymouth, USA.

Newman, J.N. 2017 Trapped-wave modes of bodies in channels. *J. Fluid Mech.* **812**, 178–198.

Porter, R 2018 Trapping of waves by thin floating ice floes. *Q. J. Mech. Appl. Maths* **71**, 463–483.

Ren, K., Wu, G.X. & Ji, C.Y. 2018 Wave diffraction and radiation by a vertical circular cylinder standing in a three-dimensional polynya. *J. Fluids Struct.* **82**, 287–307.

Ren, K., Wu, G.X. & Thomas, G.A. 2016 Wave excited motion of a body floating on water confined between two semi-infinite ice sheets. *Phys. Fluids* **28**, 127101.

Riska, K., Lohi, P. & Eronen, H. 2005 The width of the channel achieved by an azimuth thruster icebreaker. In *The 18th International Conference on Port and Ocean Engineering under Arctic Conditions*. 26–30 June, New York, USA.

Robin, G.Q. 1963 Wave propagation through fields of pack ice. *Phil. Trans. R. Soc. Lond.* A **255**, 313–339.

Squire, V.A. 2011 Past, present and impendent hydroelastic challenges in the polar and subpolar seas. *Phil. Trans. R. Soc. Lond.* A **369**, 2813–2831.

Squire, V.A., Dugan, J.P., Wadhams, P., Rottier, P.J. & Liu, A.K. 1995 Of ocean waves and sea ice. *Annu. Rev. Fluid Mech.* **27**, 115–168.

Squire, V.A., Robinson, W.H., Langhorne, P.J. & Haskell, T.G. 1988 Vehicles and aircraft on floating ice. *Nature* **333**, 159–161.

Srokosz, M.A. & Evans, D.V. 1979 A theory for wave-power absorption by two independently oscillating bodies. *J. Fluid Mech.* **90**, 337–362.

Sturova, I.V. 2015 Radiation of waves by a cylinder submerged in water with ice floe or polynya. *J. Fluid Mech.* **784**, 373–395.

Timoshenko, S.P. & Woinowsky, K.S. 1959 *Theory of Plates and Shells*. McGraw-Hill.

Ursell, F. 1951 Trapping modes in the theory of surface waves. *Math. Proc. Camb. Phil. Soc.* **47**, 347–358.

Ursell, F. 1999 On the wave motion near a submerged sphere between parallel walls: I. Multipole potentials. *Q. J. Mech. Appl. Maths* **52**, 585–604.

WEHAUSEN, J.V. & LAITONE, E.V. 1960 *Surface Waves*, pp. 446–778. Springer.
WILLIAMS, T.D. & SQUIRE, V.A. 2006 Scattering of flexural–gravity waves at the boundaries between three floating sheets with applications. *J. Fluid Mech.* **569**, 113–140.
WU, G.X. 1998 Wave radiation and diffraction by a submerged sphere in a channel. *Q. J. Mech. Appl. Maths* **51**, 647–666.
YEUNG, R.W. & SPHAIER, S.H. 1989 Wave-interference effects on a truncated cylinder in a channel. *J. Engng Maths* **23**, 95–117.